Atmos. Chem. Phys., 26, 5813–5837, 2026
https://doi.org/10.5194/acp-26-5813-2026

Atmospheric Chemistry and Physics
Open Access
EGU

Research article

Sources, concentrations, and seasonal variations of VOC and aerosol particles in downtown Munich in 2023/2024

Yanxia Li[1], Hengheng Zhang[1,a], Xuefeng Shi[1], Yaowei Li[2,b], Sophie Abou-Rizk[2], Jessica B. Smith[2], Zhaojin An[2,c], Adrian Wenzel[3], Junwei Song[4], Thomas Leisner[1,5], Frank Keutsch[2], Jia Chen[3], and Harald Saathoff[1]

[1]Institute of Meteorology and Climate Research-Atmospheric Aerosol Research, Karlsruhe Institute of Technology, 76344 Eggenstein-Leopoldshafen, Germany
[2]Paulson School of Engineering and Applied Sciences, Harvard University, Cambridge, MA 02138, USA
[3]Environmental Sensing and Modeling, Technical University of Munich (TUM), Munich, Germany
[4]Irceylon, Universite Claude Bernard Lyon 1, CNRS, UMR 5256, 69100 Villeurbanne, France
[5]Institute of Environmental Physics, Heidelberg University, 69120 Heidelberg, Germany
[a]now at: Research Institute for Applied Mechanics, Kyushu University, Fukuoka, Japan
[b]now at: Department of Earth, Atmospheric, and Planetary Sciences, Massachusetts Institute of Technology, Cambridge, MA 02139, USA
[c]now at: School of Environment, Tsinghua University, 10084, Beijing China

Correspondence: Yanxia Li (yanxia.li@kit.edu) and Harald Saathoff (harald.saathoff@kit.edu)

Received: 20 October 2025 – Discussion started: 20 November 2025
Revised: 10 March 2026 – Accepted: 10 April 2026 – Published: 29 April 2026

Abstract. Little is known about molecular composition and sources of air pollution in Germany's third largest city, Munich. Therefore, we investigated sources, concentrations, and seasonal variations of volatile organic compounds (VOC), semi-volatile organic aerosol (SVOA), and organic aerosol (OA) in an urban street canyon in Munich utilizing online mass spectrometry and positive matrix factorization (PMF). Organic aerosol concentrations were higher in summer ($4.3 \pm 2.9\,\mu g\,m^{-3}$) than late winter ($3.3 \pm 1.7\,\mu g\,m^{-3}$), consistent with enhanced photochemical reactions, while nitrate exhibited the opposite trend with elevated concentrations in winter ($4.5 \pm 3.2\,\mu g\,m^{-3}$) compared to summer ($0.3 \pm 0.2\,\mu g\,m^{-3}$). During summer heat, photochemistry is associated with the formation of low-volatile oxygenated OA ($33 \pm 20\,\%$), while aged biomass burning organic aerosol (BBOA) ($25 \pm 21\,\%$) associated with barbecue activities and biogenic OA ($22 \pm 14\,\%$) linked to nocturnal monoterpene chemistry further shape aerosol composition. The colder seasons are characterized by combustion-derived aerosols (Winter: fresh BBOA $13 \pm 9\,\%$, aged $36 \pm 12\,\%$; Spring: fresh $27 \pm 17\,\%$, aged $37 \pm 19\,\%$), whose dynamics are driven mainly by anthropogenic activity patterns. Traffic contributed at this urban kerbside relatively little to aerosol mass (5 %–9 %) but more to VOC (22 %–35 %). Our findings point to potential strategies to improve air quality e.g. by reducing monoterpene emissions by urban vegetation management as well as reducing biomass burning including barbecue emissions, which are attributed to a substantial fraction of aerosol particles and precursor gases of secondary organic aerosol throughout the seasons.

Published by Copernicus Publications on behalf of the European Geosciences Union.

1 Introduction

Volatile organic compounds (VOC) and organic aerosols (OA) are major components of urban air pollution, contributing to the formation of secondary pollutants like ozone and secondary organic aerosol (SOA), which pose significant risks to air quality, climate, and human health (Wu et al., 2020; Nault et al., 2021; IPCC, 2023). Moreover, different weather conditions and seasons influence the dispersion, deposition, and transformation of these pollutants (Crippa et al., 2013; Debevec et al., 2021; Stirnberg et al., 2021). Identifying SOA sources is crucial for reducing complex observational datasets to key real-world contributors, enabling timely air quality management, policy evaluation, and accurate air pollution forecasting (Chen et al., 2022a). However, pinpointing the sources of SOA is particularly challenging due to its composition as a highly complex mixture of largely unidentified compounds, coupled with the complicated and multistep transformation processes of VOC into SOA (Daellenbach et al., 2019).

The high-resolution time-of-flight Aerodyne aerosol mass spectrometer (HR-TOF-AMS, Aerodyne Research Inc., Billerica, MA, USA) quipped with a $PM_{2.5}$ aerodynamic lens is used for the online characterization of non-refractory $PM_{2.5}$. Positive matrix factorization (PMF) analysis of AMS datasets can quantitatively resolve major primary organic aerosol (POA) sources, including traffic-related hydrocarbon-like organic aerosol (HOA) and biomass burning organic aerosol (BBOA) (Chakraborty et al., 2017; Lalchandani et al., 2021). However, AMS datasets cannot specify sources for secondary organic aerosol (SOA) due to significant fragmentation from thermal volatilization ($\sim$ 600 °C) and harsh electron impact ionization ($\sim$ 70 eV) (Qi et al., 2020; Kumar et al., 2022). Additionally, without information on VOC as SOA precursors, it is difficult to attribute SOA factors – e.g., semi-volatile oxygenated OA (SV-OOA) and low-volatility oxygenated OA (LV-OOA) – to specific sources or formation mechanisms using AMS-PMF analysis (Song et al., 2024). Proton transfer reaction time-of-flight mass spectrometry (PTR-TOF-MS) is a useful tool to identify the sources of VOC and oxygenated VOC (OVOC), and in elucidating their contributions to the SOA formation (Wang et al., 2020a; Pfannerstill et al., 2019). Furthermore, the CHARON-PTR-MS (Chemical Analysis of Aerosol Online Particle Inlet coupled to a PTR-TOF-MS) is a continuous measurement technique capable of providing molecular-level chemical characterization and time-resolved quantification of semi-volatile organic aerosol components (Eichler et al., 2015; Müller et al., 2017; Piel et al., 2019). CHARON-PTR-MS enhances the detection of detailed SOA chemical composition data by minimizing thermal decomposition and ionization-induced fragmentation compared to AMS employing high-temperature vaporization and electron-impact ionization (Gkatzelis et al., 2018b; Leglise et al., 2019). This is achieved through lower thermal stress during particle evaporation at reduced pressure and softer chemical ionization via proton-transfer reactions, which better preserves molecular information.

Huang et al. (2019) found that in the city of Stuttgart (southwest Germany) SOA from VOC oxidation dominated the organic aerosol burden, with primary sources like traffic contributing less, while residential wood burning became particularly important during winter in residential areas. A study in downtown Karlsruhe (southwest Germany) demonstrated that secondary oxygenated OA comprised over 60 %–75 % of total OA throughout the year, with primary traffic-related OA showing seasonal variations and wood combustion becoming more significant during cold periods under stagnant meteorological conditions (Song et al., 2022). A Europe-wide analysis revealed that oxygenated OA (secondary formation) accounted for an average of 71 % of submicron OA mass across 22 sites, with solid fuel/biomass burning contributing 16 % and primary urban sources (traffic, cooking) typically less than 10 %–15 % (Chen et al., 2022b). These findings underscore the necessity for site-specific OA and VOC source apportionment studies in major European cities such as Munich in southern Germany. Although secondary formation processes consistently dominate regional OA burdens, the underlying VOC precursors, and primary emission contributions exhibit substantial spatial and temporal variability.

Munich, the capital of Bavaria, Germany, is a major cultural and economic center with a population of 1.5 million as of 2023, making it the third-largest city in Germany. It has a population density of 4700 people per square kilometers (München, 2023). Despite significant progress in air quality regulations, Munich still struggles with aerosol pollution. Identifying the sources of VOC and particulate matter is crucial for improving air quality in Munich. However, there have been only a limited number of studies characterizing aerosols in Munich. Schnelle-Kreis et al. (2001) collected filters from three traffic-dominated sites and one additional site located on the northern outskirts of Munich, approximately 1 km from the city center, between 1996 and 1998. Using HPLC analysis, they found that 40 % of polycyclic aromatic hydrocarbons (PAHs) were associated with fine particles. Schäfer et al. (2011) monitored air pollution across Munich and its outskirts, employing long-term as well as campaign-based monitoring stations from LfU (Bayerisches Landesamt Für Umwelt), Meteorological Institute of the Ludwig-Maximilians-University Munich (MIM), and IMK-IFU (e.g., Maisach) covering traffic-related (e.g., Lothstraße, Stachus, Luise-KiesselbachPlatz), urban (MIM), and suburban (Johanneskirchen) sites, during campaigns in late spring (10–30 May 2003) and winter (27 November–15 December 2003). They found higher particle mass concentrations at the urban site compared to rural areas, especially in winter, with no significant differences in major ionic composition between the sites (Schäfer et al., 2011). Qadir et al. (2013) identified traffic, cooking, solid fuel combustion, and mixed

aerosols (from tobacco smoke, cooking, and wood combustion) as the primary sources of aerosols at Lothstraße in Munich during the winter periods of October 2006 to February 2007 and October 2009 to February 2010. Schnell (2014) identified biomass burning aerosol as the dominant aerosol type at the rural site of Maisach and the urban site of MIM during the winter seasons from 2007 to 2010. Recently, a study on aerosol emissions from Munich Airport showed its impact in the outskirts of Munich, especially for ultrafine particles (UFPs) (Seidler et al., 2024). Despite these previous studies, we still have limited understanding of the main sources of VOC and OA through concurrent online measurements, their typical concentration levels across seasons, and their seasonal variations in molecular composition in Munich. It remains unclear how much anthropogenic and biogenic sources contribute to organic aerosol in Munich and what is the fraction of biomass burning aerosol originates from residential wood combustion versus barbecue activities. Therefore, we examined in this study the seasonal variability of OA and VOC chemical composition at a molecular level in a street canyon (Theresienstrasse 39) in downtown Munich, aiming to elucidate the contribution of different sources to major VOC, SVOA, and total OA concentrations. The $PM_{2.5}$ concentrations at the Theresienstrasse were measured using a FIDAS 200 optical particle spectrometer (Palas GmbH, Germany) and are comparable to those observed at the regulatory monitoring station Munich/Stachus of LfU (LfU Bayern, 2025). For 2023, the annual average $PM_{2.5}$ concentration at the reference station was $9.3 \pm 6.2\,\mu g\,m^{-3}$, with August showing $8.7 \pm 5.7\,\mu g\,m^{-3}$, compared to our measured value of $6.7 \pm 3.7\,\mu g\,m^{-3}$. In 2024, the annual average at the reference station was $8.7 \pm 6.6\,\mu g\,m^{-3}$, with March averaging $9.0 \pm 9.9\,\mu g\,m^{-3}$, while our March measurements yielded $8.7 \pm 9.2\,\mu g\,m^{-3}$. Both measurement periods demonstrated strong correlations ($R = 0.8$) (Fig. S1 in the Supplement). The close agreement between our measurements and the official monitoring data, combined with the high correlation coefficients, validates the representativeness of our sampling location for characterizing the urban downtown atmosphere in Munich. Please note that this work is linked to the recently established low-cost sensor network in downtown Munich, monitoring especially O_3, NO_2, and $PM_{2.5}$ (Wenzel et al., 2025). For our dedicated source apportionment, we conduct separate statistical analyses on VOC from PTR-TOF-MS, SVOA from CHARON-PTR-MS, and OA from HR-TOF-AMS to identify the sources of VOC, SVOA, and OA from their chemical fingerprints.

2 Methodology

2.1 Measurement location

Field observations were conducted during three meteorological periods: summer (3–29 August 2023), late winter (1–8 March 2024), and spring (9–27 March 2024). The separation between winter and spring periods was based on observed transitions in ambient temperature and chemical composition, including systematic changes in organic aerosol and nitrate concentrations observed in the time series (Figs. 1d and 2), indicating a shift from colder, nitrate-favored conditions to warmer conditions associated with enhanced photochemical activity. Spring conditions were characterized by higher solar radiation and an increased relative contribution of organic aerosol (Figs. 1d and 2), reflecting stronger photochemical production. These periods therefore represent meteorologically and chemically distinct regimes rather than strict calendar-based seasonal classifications. The sampling site (11°57′ E, 48°15′ N) was located on a parking lot next to a 30 m tall building of the Ludwigs-Maximilians-University (LMU) of Munich in a street canyon of Theresienstrasse 39 (Fig. S2). The elevation on street level at this location is 520 m a.s.l. The street has several restaurants, apartment buildings, museums, university workshops, laboratories, and substantial vehicular traffic. The wind direction at the site in the street canyon predominantly originates from the south and southeast due to a vortex due to upwind or lee side of the LMU building. At the rooftop of the 30 m LMU building, it mainly came from the west and east. Wind speed and direction exhibit minimal variation for the measurement periods (Fig. S2).

2.2 Instrumentation

An overview of all instruments used in this campaign to characterize aerosol particles, trace gases, and meteorological parameters is provided in Table S1 in the Supplement. The major instruments used are described in more detail below.

2.2.1 CHARON-PTR-TOF-MS

A proton-transfer-reaction time-of-flight mass spectrometer (PTR-ToF-MS 4000X2, Ionicon Analytik GmbH), equipped with a particle inlet (Chemical Analysis of aeRosol ONline, CHARON), was utilized to measure VOC in the gas phase and semi-volatile compounds in the particle phase. The PTR-ToF-MS 4000X2 employed here has an ion funnel, which reduces ion loss and enhances sensitivity (Pugliese et al., 2020). The CHARON inlet integrates a gas-phase denuder, an aerodynamic lens with an inertial sampler, and a thermodesorption unit, all coupled to a PTR-TOF-MS. The gas-phase denuder removes gas-phase analytes, while the aerodynamic lens focuses the aerosol particles. The inertial sampler then concentrates the particle-enriched sample flow. Finally, the particles enter a thermal desorption unit where they are volatilized before being detected by PTR-MS. The inlet system demonstrated a particle enrichment factor of 18 ± 2 (Fig. S3), as discussed in detail in our previous study (Song et al., 2024). The vaporizer (TDU) was operated at 150 °C and 7–8 mbar absolute pressure. The CHARON inlet was de-

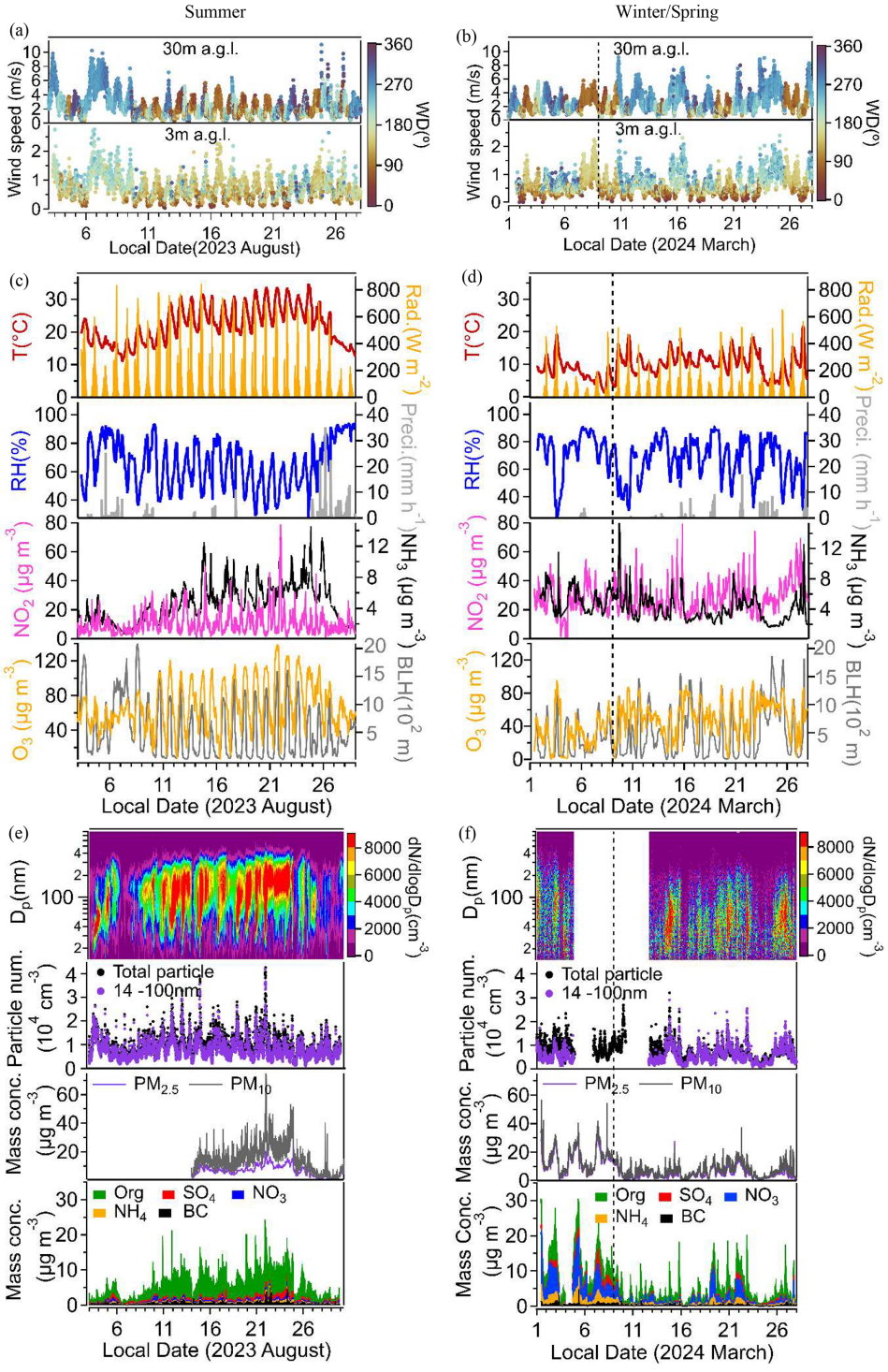

Figure 1. Time series of wind speed and direction 3 and 30 m a.g.l. (above ground level) in summer **(a)** and winter **(b)**; temperature (T); global radiation (Ra); relative humidity (RH); precipitation; NO_2; NH_3; O_3 and boundary layer height (BLH*) in summer **(c)** and winter **(d)**; particle number size distributions; particle number of total and below 100 nm ultrafine particles; $PM_{2.5}$ and PM_{10} mass concentrations; organic aerosol (OA), sulfate, nitrate, and ammonium; Equivalent black Carbon (eBC) in summer **(e)** and **(f)** in winter; # All data plotted except the wind data were measured at the container roof. *Please note that the BLH data refer to ERA5 reanalysis data (Guo et al., 2024), which represent large-scale boundary layer conditions and may not fully capture street-canyon ventilation or local turbulence effects. The vertical dotted line marks the transition between the late-winter and early-spring periods, defined based on observed changes in temperature, solar radiation, and aerosol chemical composition.

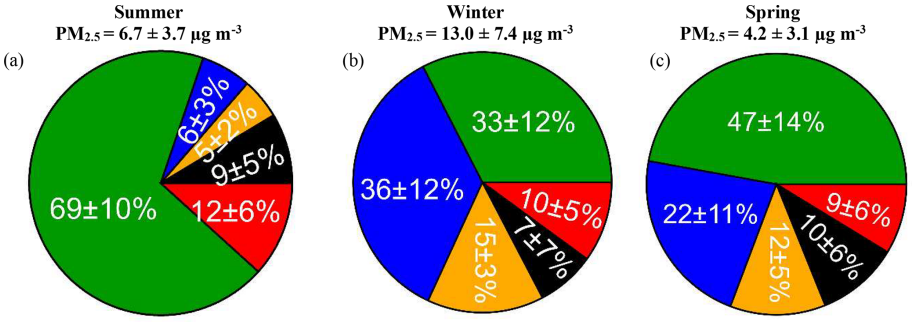

Figure 2. Average fractions of $PM_{2.5}$: OA (green), sulfate (red), nitrate (blue), ammonium (yellow) and eBC (black) in summer **(a)**, **(b)** in winter (until 8 March) and **(c)** in spring based on AMS and Aethalometer measurements.

scribed in detail elsewhere (Eichler et al., 2015; Müller et al., 2017; Gkatzelis et al., 2018a; Gkatzelis et al., 2018b).

In this campaign, the CHARON-PTR-MS automatically switched between gas and particle phase measurements. The sequence was: 5 min of high-efficiency particulate air (HEPA) filter measurement for particle background, 10 min of particle-phase measurement, 3 min transition, 10 min of gas-phase VOC measurement, and another 2 min transition. The PTR drift tube was kept at 2.7 mbar, 470 V, and 100 °C, with the ion funnel at 45 V. These settings correspond to an electric field (E) to gas molecule number density (N) ratio of ∼ 100 Td for VOC measurement. For particle measurement, the PTR was automatically adjusted to 60 Td.

During gas-phase measurement, ambient air was sampled continuously from a 2 m PFA tube (4 mm inner diameter) at 8 L min^{-1}, with 40–100 mL min^{-1} directed to the PTR-ToF-MS through a polyetheretherketone (PEEK) tubing at 80°. The instrumental background was determined weekly at noon by introducing pure dry nitrogen (N_2, 99.9999 %) into the inlet for 5–15 min to exclude ambient air and quantify the instrumental baseline (Fig. S4). For particle-phase measurement, ambient particles were sampled with a $PM_{2.5}$ inlet (Comde Dendra) through a vertical electropolished 3.45 m stainless-steel tube (12 mm inner diameter) at 16.7 L min^{-1}, with 550 mL min^{-1} directed to the CHARON inlet. Particle background was automatically determined using the HEPA filter.

Gas calibrations were performed at the beginning, middle, and end of each campaign periods using a gas cylinder (Ionicon Analytik GmbH) with 15 VOC, including toluene, trimethylbenzene, xylene, alpha-pinene, acetone, acetonitrile, benzene, and isoprene (accuracy 5 % at ∼ 1000 ppb). The sensitivity ranged from ∼ 1000 to 4000 cps ppb^{-1} for different compounds across different seasonal calibration periods (Fig. S5). Raw data from CHARON-PTR-MS were processed using IONICON Data Analyzer software (IDA 2.2.0) following Müller et al. (2013), Lannuque et al. (2023), and Peron et al. (2024). The CHARON inlet enrichment factor was determined via external calibration with size-selected (DMA, TSI) ammonium nitrate particles (100–500 nm) measured by a condensation particle counter (CPC, TSI).

2.2.2 HR-TOF-AMS

A high-resolution time-of-flight Aerosol Mass Spectrometer (HR-ToF-AMS) (Aerodyne Research Inc.), equipped with a $PM_{2.5}$ aerodynamic lens, was used to measure non-refractory $PM_{2.5}$ (NR-$PM_{2.5}$) components, including organic aerosol, nitrate, sulfate, ammonium, and chloride, with a time resolution of 1 min (DeCarlo et al., 2006; Canagaratna et al., 2007; Williams et al., 2013). The operation and calibration procedures of the AMS are detailed in our previous publications (Huang et al., 2019; Song et al., 2022). The instrument's capability to provide high-resolution mass spectra enables detailed chemical composition analysis of aerosol particles in real time. Briefly, ambient air was sampled through a $PM_{2.5}$ inlet (flow rate of 1 m^3 h^{-1}) that was shared with the CHARON system via a 3.45 m stainless-steel tube. A subset of this flow was then directed to the HR-ToF-AMS at a flow rate of 84 cm^3 min^{-1}. The aerosol particles were focused into a narrow beam by a $PM_{2.5}$ aerodynamic lens, which effectively transmits particles with vacuum aerodynamic diameters (dva) ranging from ∼ 70 to ∼ 2500 nm. The particles were subsequently heated by a vaporizer at 600 °C, causing the non-refractory components to volatilize. The volatilized particles were then ionized by electron impact at 70 eV, which is a standard method for ionizing organic and inorganic compounds, ensuring fragmentation patterns that are well-characterized and suitable for identification. The AMS was calibrated using dried ammonium nitrate aerosol particles with sizes of 100–500 nm to determine ionization efficiency and instrument response. Calibration particles were size-selected using a DMA, and signal stability was verified prior to and during each measurement period. Data from the AMS were processed and analyzed using the SQUIRREL 1.65G and PIKA 1.25G software packages. To address the issue of particle bounce losses, a chemical-composition-based collection efficiency (CE) of

approximately 0.5 was applied to calculate the particle mass concentrations (Docherty et al., 2011; Middlebrook et al., 2012). For the elemental analysis of organic aerosol (OA), including the hydrogen-to-carbon ratio (H : C) and the oxygen-to-carbon ratio (O : C), we utilized the improved ambient method (Aiken et al., 2008; Canagaratna et al., 2015).

2.2.3 Other instruments

The mass concentrations of $PM_{2.5}$ and PM_{10} and particle size distributions (0.2–18 µm) were determined using an optical particle counter (Fidas200, Palas). Particle number concentrations (> 2.5 nm) were monitored using a water-based condensation particle counter (Model 3789, TSI Inc.) and a butanol-based condensation particle counter CPC3776 (TSI Inc., USA). Particle number size distributions ranging from 10 to 410 nm were measured using a nanoparticle sizer (Nanoscan 3910; TSI Inc.) at time resolution of 1 min in winter, and distributions ranging from 13.6 to 763.5 nm were measured using a scanning mobility particle sizer (SMPS; DMA 3081; TSI Inc.) at a time resolution of 7 min in Summer. Equivalent black carbon (eBC) levels were monitored with an aethalometer (AE33, Magee Scientific) at a 1 min resolution. Ammonia (NH_3) concentrations were measured via cavity ring-down spectroscopy (G2103, Picarro Inc.). The gas was sampled via a Teflon tube (4 mm i.d.; 3.1 s residence time). Ozone (O_3) and nitrogen dioxide (NO_2) concentrations were tracked using the $O_3$41M and AS32M gas analyzers (both from Environment S.A.), respectively. Meteorological parameters such as temperature, relative humidity, wind speed and direction, global radiation, and precipitation were recorded with a compact weather sensor (WS700, Lufft) installed on the container roof. Additional meteorological data was measured by the Institute of Meteorology of the LMU on top of the institute at about 30 m a.g.l. (https://www.meteo.physik.uni-muenchen.de/request-beta/, last access: 23 April 2026). The vertical aerosol distribution was assessed using a scanning aerosol Lidar (Rametrics Inc., Type: LR111-ESS-D200, named KASCAL). Fiber laser-induced fluorescence (FILIF) detects formaldehyde (HCHO) by exciting molecules at 353 nm and measuring fluorescence above 370 nm. The technique alternates between on-peak and off-peak laser frequencies to determine HCHO concentration with high specificity. Calibrated against FTIR standards, FILIF achieves ±27 pptv precision (10 %–15 % accuracy) at 10 Hz sampling frequency, unaffected by humidity. All the information could be found in previous studies (Ye et al., 2021). Unless otherwise specified, all measured values are reported as mean ± standard deviation. Please note that this work is linked to the recently established low-cost sensor network in downtown Munich, monitoring especially O_3, NO_2 and $PM_{2.5}$ (Chen, 2025). This included frequent comparison measurements between reference instruments on a bicycle platform, the instruments in our container, a LfU regulatory monitoring station, and the low-cost sensor network in downtown Munich. Back trajectories were calculated using the Hybrid Single-Particle Lagrangian Integrated Trajectory (HYSPLIT) model (Stein et al., 2015) at 500 m altitude with 72 h backward duration to identify potential source regions and transport pathways influencing air quality at the measurement site.

2.2.4 PMF analysis

The PMF receptor model is a bilinear algorithm that separates air pollutant time series into sources characterized by factor profiles, time series, and residuals (Paatero and Tapper, 1994; Paatero, 1999). It is widely used to identify particle and VOC sources (Kim et al., 2004; Reyes-Villegas et al., 2016; Huang et al., 2018; Gkatzelis et al., 2021).

PMF has also been applied to inorganic aerosol components, elemental composition of particulate matter (PM), VOC, PAHs, black carbon, and size-resolved particle data, showing its versatility as a receptor model across various pollutant types (Äijälä et al., 2019). PMF has been used for analyzing high-time-resolution elemental data in $PM_{2.5}$ and PM_{10} to identify urban and industrial sources and to separate fine and coarse particle sources (Reizer et al., 2021). Reviews and guidelines from European air quality agencies explicitly mention the use of PMF applied to particle mass, ions, metals, and gaseous species (like VOC and PAHs) in addition to OA for comprehensive source apportionment studies (Belis et al., 2013). In summary, PMF receptor modeling is broadly used and suitable for source apportionment of multi-pollutant data sets.

To investigate the sources of VOC, SVOA, and OA, positive matrix factorization (PMF) was applied separately to (i) VOC mass spectra measured by PTR-MS, (ii) semi-volatile aerosol species measured by CHARON-PTR-MS, and (iii) OA measured by HR-TOF-AMS. PMF analyses were conducted independently for each dataset and measurement campaign rather than using a combined dataset. Separate analyses were chosen because the campaigns were performed in different seasons under substantially different atmospheric conditions and instrument states. PMF assumes temporally stationary factor profiles and comparable uncertainty structures within a dataset; these assumptions are not fulfilled when combining measurements across seasons with distinct source contributions and atmospheric processing regimes. In addition, VOC and SVOA datasets were analyzed separately because they represent chemically and physically distinct phases with different atmospheric processing timescales, variability patterns, and measurement uncertainty structures. Combining these datasets in a single PMF analysis would violate the assumption of consistent covariance structure and could lead to mixed or non-interpretable factors. Diagnostic evaluations supporting solution stability and factor selection for each dataset are provided in the Supplement (Figs. S8–S20). For VOC-PMF, inputs were derived from PTR-TOF-MS data following the methodology of Song

et al. (2024), involving comprehensive preprocessing including mass spectral deconvolution, background subtraction, and error matrix calculation where uncertainties were determined as $[(0.1 \times \text{concentration})^2 + (0.5 \times \text{LOD})^2]^{1/2}$ (Kajos et al., 2015). SVOA-PMF inputs were obtained through two complementary measurement modes: HEPA-filtered air samples (representing background signals) and direct atmospheric sampling (Dir) capturing real-time conditions, with ions (primarily $C_xH_y^+$, $C_xH_yO_z^+$, and $C_xH_yO_zN_n^+$). Both datasets underwent rigorous quality control procedures. Low-molecular-weight species ($m/z \leq 60$) were excluded to eliminate potential interferences from fragments and common atmospheric gases that may not be representative of specific emission sources (Zhang et al., 2011). Additionally, compounds with $\geq 20\,\%$ missing data points were removed to ensure statistical robustness in the PMF analysis, following established protocols for PMF data preparation (Ulbrich et al., 2009; Zhang et al., 2011). The analyses were initially processed using SoFi Pro 9.0 (Datalystica Ltd.) for exploratory factor analysis and data visualization. The source apportionment of organic aerosols (m/z12–120) was then conducted through unconstrained AMS-PMF analysis using the PMF Evaluation Tool (v3.08C) within IGOR Pro (v8.04), which maintains legacy algorithms specifically optimized for AMS datasets, particularly for handling nonlinear m/z signal-uncertainty relationships in typical AMS operating conditions.

The final number of factors for each dataset was selected based on a combination of diagnostic criteria, including the evolution of Q/Q_{exp} values, inspection of scaled residual distributions, physical interpretability of factor profiles, and temporal behavior. Physical interpretability was evaluated using dominant marker compounds in each factor mass spectrum together with their temporal patterns, allowing source attribution based on established source signatures (e.g., traffic-related factors identified by toluene/xylene dominance and rush-hour diurnal peaks). Solutions with increasing factor numbers were examined to identify the point beyond which additional factors primarily resulted in factor splitting without meaningful improvement in residual structure. Detailed diagnostics, including Q/Q_{exp} evolution, residual analysis, Fpeak sensitivity tests, and correlations with characteristic compound markers and diurnal patterns, are provided in the Supplement (Sect. S3.2, Figs. S7–S19, Table S4–S9).

3 Results and discussion

In the first section, we give an overview of the meteorological conditions during the two measurement campaigns and the main characteristics of the observed evolution of aerosol particles and trace gases. The second section will discuss the major sources of aerosol particles and trace gases. In the third section, we focus on strong biomass burning events.

3.1 Overview of observations during summer and wintertime

3.1.1 Overview of meteorological and particle observations

The summer period was characterized by frequent sunny weather with moderate to high temperatures and significant precipitation events mainly at the beginning and end of the summer campaign. The late winter/spring period shows typical winter conditions until 8 March, according to temperature, precipitation followed by more spring-like conditions thereafter.

Wind measurements at 3 and 30 m above ground (Fig. 1a and b) revealed consistent vertical gradients across all seasons, with average speeds of 0.7 ± 0.4 and $2.6 \pm 1.4\,\text{m s}^{-1}$, respectively. Meteorological conditions varied significantly between seasons (Fig. 1c and d), creating distinct chemical environments. The higher summer temperatures ($21.9 \pm 5.8\,^{\circ}\text{C}$) promoted enhanced biogenic emissions and photochemical activity, while lower winter temperatures ($8.4 \pm 3.0\,^{\circ}\text{C}$) favored primary pollutant accumulation. Relative humidity and total precipitation showed minimal seasonal variation. NO_2 concentrations were 2.5–2.8 times higher in winter/spring ($26.1 \pm 9.9/28.4 \pm 10.8\,\mu\text{g m}^{-3}$) than summer ($10.2 \pm 7.7\,\mu\text{g m}^{-3}$) due to increased heating emissions and reduced photolysis under shallow boundary layers (339 ± 298 m/510 ± 477 m vs. 516 ± 453 m, variability). The BLH values are derived from ERA5 reanalysis and represent regional-scale atmospheric mixing. They do not resolve street-canyon ventilation. In a street canyon, buildings can limit horizontal and vertical dispersion, especially under stable winter conditions. Therefore, pollutant accumulation at the measurement site may be stronger than suggested by ERA5 BLH alone. This limitation is particularly relevant for reactive pollutants such as NO_2. In addition to dispersion, NO_2 is strongly influenced by local traffic emissions and rapid photochemical processes (e.g., photolysis and O_3 titration). As a result, short-term variations in NO_2 may reflect a combination of street-canyon trapping, advection, and chemical transformation. This can differ from more inert traffic-related species such as BC, which are primarily governed by physical mixing. The ERA5 BLH should therefore be interpreted as an indicator of large-scale mixing conditions rather than street-level ventilation. The LfU station showed similar winter ($27.2 \pm 9.2\,\mu\text{g m}^{-3}$) and early spring ($27.8 \pm 9.2\,\mu\text{g m}^{-3}$) mean concentrations to Theresienstrasse, but exhibited weak temporal correlation, reflecting the strong spatial variability of NO_2. Notably, summer NO_2 at LfU ($23.4 \pm 10.1\,\mu\text{g m}^{-3}$) was 2.3 times higher than Theresienstrasse, yet temporal correlation improved substantially ($R = 0.5$) in Fig. S6. This seasonal pattern suggests that summer's higher boundary layer enhanced vertical mixing and local photochemical reactions, increasing spatial differences in mean NO2 levels. However, stronger

synchronized daily photochemical cycles improved temporal agreement between the two sites. The diurnal evolution of NO_2, O_3, and BLH reveals seasonally distinct coupling between photochemical processing and boundary-layer mixing (Fig. S7). During summer, increasing BLH coincides with decreasing NO_2 concentrations and enhanced daytime O_3 formation, indicating efficient vertical mixing and active photochemical processing. Spring exhibits intermediate behavior, whereas winter shows weaker BLH development and persistently elevated NO_2 levels consistent with reduced photolysis and limited dispersion. Gaseous NH_3 showed elevated concentrations across all seasons, with winter ($5.4 \pm 1.5\,\mu g\,m^{-3}$) and spring ($4.0 \pm 1.8\,\mu g\,m^{-3}$) levels comparable to summer values ($4.8 \pm 2.6\,\mu g\,m^{-3}$). O_3 concentrations at Theresienstrasse exhibited strong seasonal variation, with highest levels in summer ($67.1 \pm 26.6\,\mu g\,m^{-3}$), followed by early spring ($52.2 \pm 19.3\,\mu g\,m^{-3}$), and lowest in late winter ($32.4 \pm 20.2\,\mu g\,m^{-3}$). The LfU station showed similar seasonal patterns (summer: $59.3 \pm 25.5\,\mu g\,m^{-3}$; late winter: $30.8 \pm 17.3\,\mu g\,m^{-3}$; early spring: $45.9 \pm 17.2\,\mu g\,m^{-3}$) with strong temporal correlations ($R = 0.8$ in August 2023; $R = 0.7$ in March 2024) in Fig. S6, indicating consistent O_3 behavior across both sites driven by regional photochemical processes.

Particle size distributions revealed contrasting seasonal patterns driven by different formation mechanisms (Fig. 1e and f). Summer showed the highest total particle number concentrations ($10\,000 \pm 5100\,cm^{-3}$) with a substantial variability dominated by ultrafine particles (< 100 nm: 80.6 ± 8.2 %), indicating a strong contribution of ultrafine particles during this period. Winter exhibited lower total number concentrations ($8900 \pm 3500\,cm^{-3}$) and a lower fraction of ultrafine particles (33.6 ± 10.1 %), consistent with a greater relative contribution of aged and accumulation-mode particles under stable conditions. Spring showed intermediate behavior with high ultrafine fractions (89.7 %) but lower absolute number concentrations. The seasonal PM mass concentrations showed opposite trends to the particle number concentrations: winter $PM_{2.5}$ peaked at $13.0 \pm 7.4\,\mu g\,m^{-3}$ with nitrate as the dominant component due to low temperatures, shallow boundary layers and increased residential heating. In contrast, summer ($6.7 \pm 3.7\,\mu g\,m^{-3}$) and spring ($4.2 \pm 3.1\,\mu g\,m^{-3}$) showed lower $PM_{2.5}$ levels dominated by organic aerosols, despite higher particle numbers, highlighting that ultrafine particles can dominate number concentrations in urban environments while contributing comparatively little to total particulate mass.

Aerosol particle mass composition varies significantly by season, reflecting different formation mechanisms. Organic aerosol particles dominate in summer due to high photochemical activity (Fig. 2), averaging $4.3 \pm 2.9\,\mu g\,m^{-3}$, higher than $3.3 \pm 1.7\,\mu g\,m^{-3}$ in winter and $1.8 \pm 1.8\,\mu g\,m^{-3}$ in spring. Nitrate is the main component in winter ($4.5 \pm 3.2\,\mu g\,m^{-3}$) due to low temperatures favoring particle phase and increased heating emissions providing abundant NH_3 and NO_x precursors for ammonium nitrate formation. Nitrate concentrations drop significantly in spring ($1.0 \pm 1.3\,\mu g\,m^{-3}$) and summer ($0.3 \pm 0.2\,\mu g\,m^{-3}$) as rising temperatures shift the equilibrium toward the gas phase. Ammonium follows similar patterns, peaking in winter ($1.8 \pm 1.1\,\mu g\,m^{-3}$) and remaining low in warmer seasons (spring: $0.4 \pm 0.4\,\mu g\,m^{-3}$; summer: $0.3 \pm 0.2\,\mu g\,m^{-3}$), consistent with reduced ammonium nitrate formation.

3.1.2 Diurnal behaviour of gaseous BVOC and BTEX

The average diurnal variations of key volatile organic compounds (VOC) are examined below, focusing on major biogenic and anthropogenic species, including BTEX – a group of aromatic hydrocarbons comprising benzene, toluene, ethylbenzene, and xylene. The VOC selected here comprise 32.3 ± 13.1 % of all VOC detected in summer, 41.0 ± 12.9 % in winter and 37.9 ± 12.5 % in spring.

Figure 3 illustrates the diurnal variations of six VOC across three seasons, revealing distinct patterns tied to their sources and environmental influences. Isoprene and monoterpenes, both biogenic VOC, exhibit the highest mixing ratios in summer. However, Isoprene displays a bimodal pattern in summer and spring, with concentration peaks during the morning and evening hours, suggesting a potential link to traffic activity during the morning and evening hours. This is consistent with direct measurements of isoprene in vehicle exhaust by Borbon et al. (2001). Additionally, fragmentation of higher-carbon aldehydes and cycloalkanes from anthropogenic sources may contribute to the signal of isoprene, further complicating source attribution in urban environments (Coggon et al., 2024b). Monoterpene exhibited early morning peaks in summer and spring, but was almost flat in winter. In contrast, their concentrations are minimal in winter due to suppressed biological activity. Anthropogenic VOC like benzene, toluene, xylene, and trimethylbenzene show different seasonal behaviors. Benzene peaks in winter, likely due to lower BLH and reduced dispersion, with dips at midday possibly from increased OH radical oxidation under sunlight. Toluene, xylene, and trimethylbenzene display notable spikes in spring, particularly during morning and evening hours, suggesting strong contributions from traffic emissions and industrial activities.

3.2 Sources of VOC and organic aerosol particles

In this section we use statistical (PMF) analysis of on-line mass spectra from VOC (PTR-MS) and semi-volatile organic aerosol particles (CHARON-PTR-MS) as well as organic aerosol particles (HR-TOF-AMS) to determine their major sources.

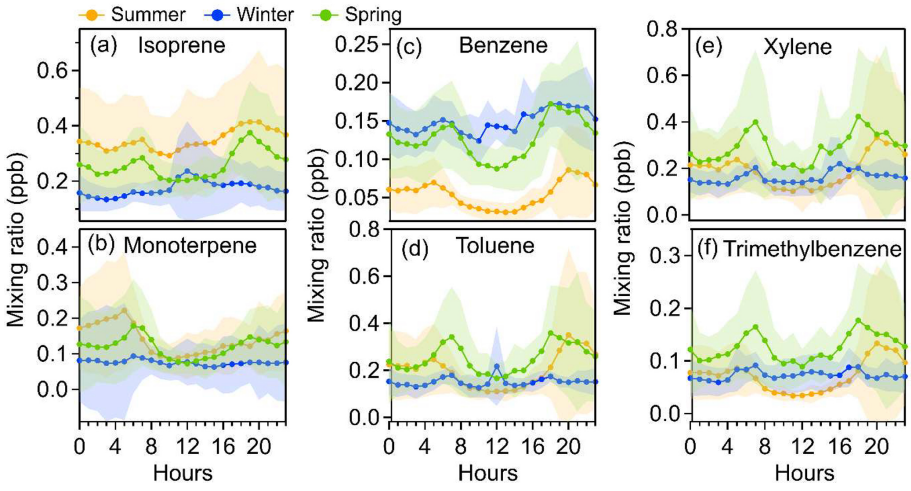

Figure 3. Diurnal behavior of **(a)** Isoprene, **(b)** Monoterpenes, **(c)** Benzene, **(d)** Toluene, **(e)** Xylene and **(f)** Trimethylbenzene in summer, winter and spring.

3.2.1 VOC sources in summer and winter

We included 117 VOC ions (Table S2) for PMF analysis in summer and 97 VOC ions (Table S3) in winter/spring. Ions with extremely high signal intensities that could disproportionately influence the PMF solution, as well as very low signal ions with minimal contribution, were excluded. The excluded high-abundance ions are common hydrocarbon and oxygenated VOC fragments, such as m/z 33.034 ($C_1H_5O^+$), 41.039 ($C_3H_5^+$), 43.054 ($C_3H_7^+$), 45.034 ($C_2H_5O^+$), 57.070 ($C_4H_9^+$), and 59.049 ($C_3H_7O^+$). These ions were removed because their high concentrations may lead to over-representation of specific factors, whereas low-signal ions were excluded to reduce noise interference (Song et al., 2024). The average VOC molecules mixing ratio is 3.4 ± 1.0 ppb in summer, 2.1 ± 0.7 ppb in winter, and 3.4 ± 1.7 ppb in spring. This study thoroughly examined factor profiles, diurnal patterns, and correlations with tracers (Figs. 4, S8 and Table S4) for summer and for winter (Figs. S9, S10 and Table S5). Five factors were identified based on measured VOC as the optimal interpretable solutions for summer and winter, respectively.

In summer, the first factor was characterized by high contributions and strong correlations with aromatic hydrocarbon ions, such as $C_7H_9^+$ (m/z 93.07), $C_8H_{11}^+$ (m/z 107.086), and $C_9H_{13}^+$ (m/z 121.102). These compounds correspond to toluene, xylenes, and C_9-aromatics, commonly used as vehicular emission markers (Squires et al., 2020; Jain et al., 2022). We assigned it to traffic VOC. These ions show a correlation coefficient (R) of approximately 0.9 with traffic emissions (Table S3). According to the diurnal profiles of traffic (Fig. 4) in summer, it shows distinct peaks during morning and evening hours.

The second factor was classified as weakly oxidized BVOC. It was identified by oxidation products of monoterpenes, specifically $C_9H_{15}O_1^+$ myrcenol (m/z 139.112), $C_{10}H_{13}O_1^+$ carvone (m/z 149.097), weakly-oxidized molecules of monoterpenes $C_{10}H_{15}O_1^+$ (m/z 151.112), $C_{10}H_{17}O_1^+$ (m/z 153.128) and $C_{10}H_{15}O_2^+$ (m/z 167.107) (Li et al., 2020a). These ions show strong correlations with the Oxidized BVOC factor, with R values of 0.93, 0.93, 0.93, 0.91, and 0.87, respectively. Oxidized BVOC have a nighttime peak in the diurnal profile and drop to nearly zero by noon, likely due to enhanced dilution and quicker oxidation to oxidation states not detectable by PTR-MS.

The third factor was identified as BVOC due to the predominance of $C_{10}H_{17}^+$ monoterpene (m/z 137.133) and its fragmentation $C_6H_9^+$ (m/z 81.07) ions in this VOC factor, with correlations of 0.98 and 0.86, respectively. Sesquiterpenes also show a strong correlation with this factor ($R = 0.80$). The average diurnal behavior of BVOC shows an early morning peak, because BVOC, especially monoterpenes, are often stored in vegetation and released at the start of the morning due to sunlight and slight temperature increases (Malik et al., 2023), combined with a shallow boundary layer that keeps emissions near the surface.

The fourth factor showed a good correlation with butyric acid $C_3H_5O_3^+$ (m/z 89.024) and $C_4H_5O_3^+$ (m/z 101.024), with R values of 0.75 and 0.72, respectively. The time series of O_3 and this factor showed a good correlation during certain periods. The diurnal cycle of it exhibits a daytime peak, indicating involvement in photochemical oxidation processes. We classified it as aged VOC.

The fifth factor, biomass burning VOC, is dominated by propylene glycol $C_3H_9O_2^+$ (m/z 77.06) and orthoacetic acid $C_2H_7O_3^+$ (m/z 79.039), with strong correlations of 0.85 and 0.83, respectively. Additionally, a ring fragment of oxidized syringol, $C_4H_7O_4^+$ (m/z 119.034), and ring fragments of oxidized guaiacol and syringol molecules $C_5H_3O_2^+$ (m/z 95.013), $C_5H_7O_4^+$ (m/z 131.034) and $C_4H_7O_3^+$

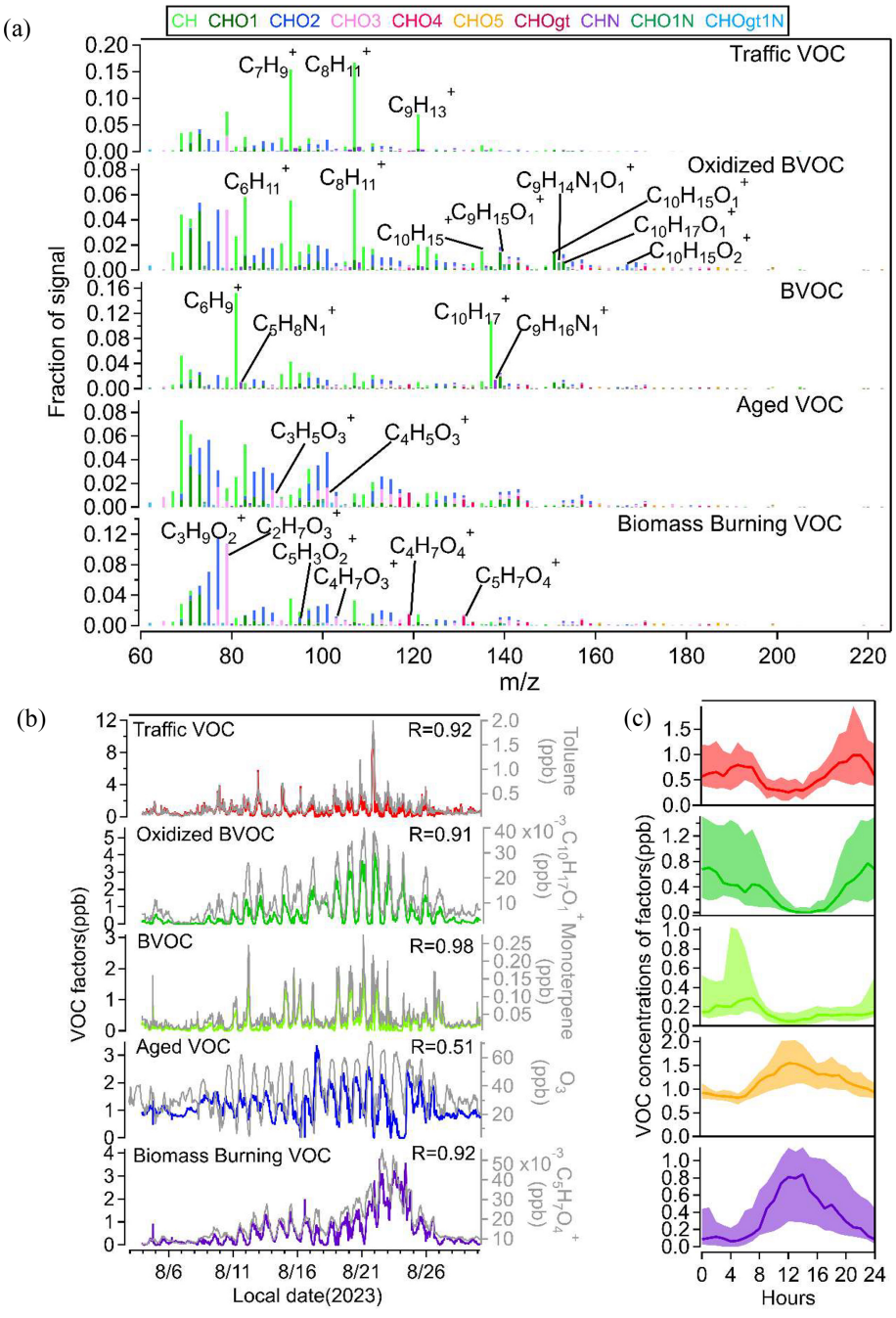

Figure 4. VOC source apportionment for summer time. **(a)** Normalized VOC factor mass spectra from PMF analysis and characteristic mass peaks in summer; **(b)** time series of VOC factors including traffic, oxidized BVOC, BVOC, aged VOC, and biomass burning VOC; **(c)** median diurnal variations in VOC factors during summer time.

(m/z 103.04) contribute smaller fractions but display even higher correlations, with values of 0.90, 0.91, 0.92 and 0.86 (Yee et al., 2013). Compared with the other 4 factors, the biomass burning VOC mass spectrum has more oxidized compounds.

In late winter and early spring, the first factor was identified as traffic VOC using the same method as in summer, showing high contributions and strong correlations with aromatic hydrocarbon ions, including toluene $C_7H_9^+$ (m/z 93.07), C_9 aromatics $C_9H_{13}^+$ (m/z 121.102), and cymene $C_{10}H_{13}^+$ (m/z 133.102) in Figs. S7, S8 and Table S5.

The second factor, classified as terpenes VOC, was marked by the predominance of monoterpene $C_{10}H_{17}^+$ (m/z 137.133) and its fragment $C_6H_9^+$ (m/z 81.07) ions with correlations

of 0.90 and 0.89, respectively. Sesquiterpenes also show a strong correlation ($R = 0.92$). The diurnal variation shows both morning and evening peaks, with the morning peak being higher than the evening peak. This pattern differs from typical traffic trends. This pattern is similar to that of limonene from shower gels (Yeoman et al., 2020), which shows higher concentrations in the morning compared to the evening. It correlates with the traffic factor because people typically shower in the morning before leaving home, leading to higher detection. By the evening, the limonene has dissipated.

The biomass burning VOC factor included a lot of smaller oxygenated VOC (OVOC) such as 1,3-propanediol $C_3H_9O_2^+$ (m/z 77.06), acetic anhydride $C_4H_7O_3^+$ (m/z 103.04), 2-furoic acid $C_5H_5O_3^+$ (m/z 113.024), maleic acid $C_4H_5O_4^+$ (m/z 117.019), butanedioic acid $C_4H_7O_4^+$ (m/z 119.034), benzoic acid $C_7H_7O_2^+$ (m/z 123.045) (Lemieux et al., 2004) and salicylic acid $C_7H_7O_3^+$ (m/z 139.04). They all show strong correlations ($R = 0.85$–0.90) with this factor. Notably, $C_5H_5O_3^+$ and $C_7H_7O_3^+$ are recognized as tracers of biomass burning VOC (Li et al., 2020b; Romanias et al., 2024). It displays a peak during the daytime, possibly due to biomass burning activities in certain areas (e.g., cooking or outdoor grilling), which increase VOC emissions and lead to a daytime peak in the VOC diurnal profile.

The fourth factor was dominated by xylene, represented by C_8-aromatic hydrocarbon $C_8H_{11}^+$ (m/z 107.086), with a correlation of 0.96. This factor also shows a strong correlation with 3-ethyl-pyridine $C_7H_{10}N_1^+$ (m/z 108.081) and the C_9-aromatic hydrocarbon VOC $C_9H_{13}^+$ (m/z 121.102), with correlations of 0.98 and 0.91, respectively. Xylene and trimethylbenzene are components of flue gases from fossil fuel combustion VOC (Niu et al., 2021). It also displays morning and evening peaks in its diurnal cycle, leading to its identification as a traffic2 VOC.

The fifth factor has minimal correlation with most masses, only showing a correlation of 0.73 with benzene ($C_6H_7^+$) and weak correlations with various oxygenated compounds. Therefore, this factor may originate from different low-concentration emission sources. Its diurnal variation shows a small evening peak, likely influenced by traffic or industrial emissions. This factor accounts for $54\,\% \pm 9\,\%$ in late winter, decreasing to $23\,\% \pm 16\,\%$ in early spring due to the increased temperature (Fig. 5), and as background VOC are commonly found to have a high proportion, we classify it as background VOC.

The source contributions of VOC vary significantly across seasons, reflecting shifts in emission patterns and atmospheric conditions. In summer, the largest contributor is aged VOC at $42 \pm 18\,\%$, indicating the dominance of secondary pollutants formed through atmospheric photochemical oxidation processing. Traffic emissions account for $22 \pm 14\,\%$, while oxidized biogenic VOC make up $13 \pm 13\,\%$, and fresh BVOC contribute $7 \pm 7\,\%$. Biomass burning plays a notable role at $16 \pm 15\,\%$, likely due to outdoor barbeque in warmer

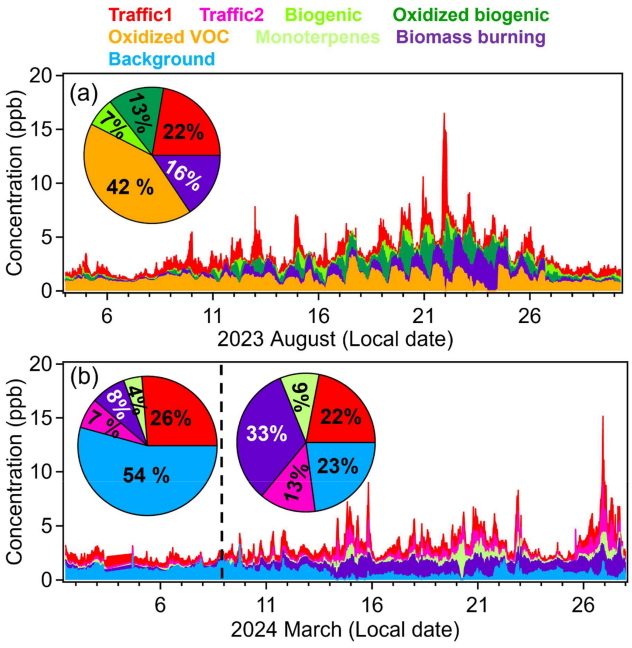

Figure 5. The time series and relative mass contribution (pie charts) of each VOC factor to total VOC concentrations in summer **(a)**, winter (left of the dash line) and spring (right of the dash line) **(b)**.

months. Winter exhibits a different profile, with background sources dominating at $54 \pm 9\,\%$, suggesting stable atmospheric conditions. Traffic-related emissions split into two categories – traffic1 ($26 \pm 6\,\%$) and traffic2 ($7 \pm 6\,\%$) – possibly reflecting different vehicle types or fuel usage patterns. Monoterpenes VOC remain low ($4 \pm 4\,\%$), consistent with reduced biogenic activity and from anthropogenic source like personal care products (Wu et al., 2024), while biomass burning contributes $8 \pm 6\,\%$, potentially from residential heating. In spring, the contributions are traffic1 $22 \pm 7\,\%$, monoterpene VOC increased to $9 \pm 9\,\%$ as vegetation becomes more active, biomass burning VOC $33 \pm 14\,\%$, traffic2 $13 \pm 8\,\%$, and background $23 \pm 16\,\%$ (Fig. 5).

3.2.2 Sources of semi-volatile organic aerosol (SVOA)

We included 153 SVOA ions (Table S6) for PMF analysis for summer and 171 SVOA ions (Table S7) for winter/spring, excluding abundant ions that could skew results and very low ion signals with minimal impact (Song et al., 2024). The average semi-volatile organic aerosol concentration was $0.3 \pm 0.2\,\mu g\,m^{-3}$ in summer, $0.14 \pm 0.08\,\mu g\,m^{-3}$ in winter and $0.07 \pm 0.07\,\mu g\,m^{-3}$in spring. Through a comprehensive analysis of factor profiles, diurnal variations, and tracer correlations in summer (Figs. S11, S12, and Table S8) and in winter (Figs. S13, S14, and Table S9). Five semi-volatile organic aerosol (SVOA) factors were identified as the best interpretable solution for different seasons.

In summer, the first factor showed distinct signals from primary oxidation products of terpenes, including oxidized monoterpenes $C_{10}H_{15}O_1^+$ ($R = 0.93$) and $C_{10}H_{17}O_1^+$ ($R = 0.89$) (Li et al., 2020a). While the expected monoterpene oxidation products are typically $C_9H_{15}O_{1-5}^+$, we found that $C_9H_{13}O_1^+$ and $C_9H_{13}O_2^+$ also correlated well with this factor, with correlation coefficients R=0.91 and R=0.85, respectively. This suggests that the $C_9H_{15}O_{1-2}^+$ compounds may lose hydrogen, forming $C_9H_{13}O_1^+$ and $C_9H_{13}O_2^+$ (Gkatzelis et al., 2018b). Additionally, nitrogen-containing species like $C_9H_{13}N_1O_1$, $C_9H_{12}N_1O_2$, and $C_9H_{13}N_1O_5$ displayed high intensity and significant correlation with this factor, which may indicate they are fragments of monoterpene-derived organic nitrates, such as $C_9H_{15}N_1O_{5-7}$ (Massoli et al., 2018). The diurnal cycle shows a nighttime peak (Fig. S10c), which we have attributed this factor to weakly oxidized biogenic organic aerosol (Weakly OBOA) based on the presence of a monoterpene oxidation tracer and the observed diurnal pattern.

The second factor includes clear markers of isoprene oxidation products, specifically $C_5H_8O_n$ species (Li et al., 2020a), with $C_5H_9O_6^+$ ($R = 0.83$) and $C_5H_9O_3^+$ ($R = 0.82$) showing strong correlations (Riva et al., 2016). Additionally, the ion with the highest fraction, $C_3H_5O_4^+$ ($R = 0.85$), likely originates from the oxidation of ISOPOOH (Rios, 2018). However, benzoic acid $C_7H_7O_2$? ($R = 0.95$), showing a strong signal, and phthalic anhydride $C_8H_5O_3^+$ ($R = 0.83$) are both known emissions from biomass burning aerosols (Bruns et al., 2017; Koss et al., 2018). $C_6H_8O_5$ ($R = 0.84$) (Molteni et al., 2018) is an oxidation product of benzene, while $C_7H_{10}O_6$ ($R = 0.84$) as reported by Nakao et al. (2011), is an oxidation product of o-cresol, an emission from oxygenated aromatic BBOA. Therefore, we define this factor as mixed oxidized isoprene OA and BBOA.

The third factor was identified as BBOA due to its strong correlation ($R = 0.88$) with vanillic acid $C_8H_8O_4$ (Fleming et al., 2020) and its prominent fragment ($C_8H_6O_4$) with even higher correlation ($R = 0.96$), which constitutes a significant portion of this factor. Additionally, another BBOA tracer, syringic acid ($C_9H_{10}O_5$) (Wan et al., 2019), and its fragment ($C_9H_6O_3$, $R = 0.95$), likely formed by the loss of two H_2O molecules, or as a direct BBOA emission (Fleming et al., 2020), further support this identification. Other ions, such as $C_6H_6O_5$ and $C_7H_8O_5$, are oxidation products of guaiacol (Yee et al., 2013). The diurnal cycle of this factor, peaking during the daytime, suggests that barbecue events may be contributing sources during the summer.

The fourth factor shows no correlation with other compounds and exhibits a distinct nighttime peak (Fig. S10c). However, it correlates strongly with nitrate detected by AMS ($R = 0.71$). This suggests that the factor represents regional background, with its nighttime increase likely influenced by local accumulation effects.

The fifth factor was identified as more oxidized monoterpene OA, comprising highly oxidized monoterpene products such as $C_{10}H_{15}O_{3-5}^+$ ($R = 0.86$, 0.85, 0.84), diacetin $C_7H_{13}O_5^+$ ($R = 0.79$), oxidized molecules of monoterpenes $C_8H_{13}O_2^+$ ($R = 0.81$), $C_8H_{13}O_4^+$ ($R = 0.80$), and its fragment ($C_8H_{11}O_3^+$, $R = 0.83$). Compounds like $C_9H_{13}O_{3-4}^+$ ($R = 0.81$, 0.78) likely arise from fragments of the $C_9H_{14}O_n$ series, representing more oxidized monoterpene products that have lost hydrogen. Compared to the diurnal pattern of less oxidized terpene products, this factor's peak displays a delay, suggesting that primary oxidation products form initially and then undergo further oxidation, resulting in more oxidized BOA (More OBOA).

In winter and spring, the first factor is identified as nighttime aged BBOA due to the presence of distinct BBOA tracers, $C_6H_6N_1O_4^+$ and $C_7H_8N_1O_4^+$ (Fig. S14a), which do not appear in the mass spectra of other factors. Nitrocatechols ($C_6H_5N_1O_4$) originates from anthropogenic activities, including biomass burning and vehicle emissions. Meanwhile, methyl-nitrocatechols ($C_7H_7N_1O_4$) are specific markers for BBOA, as they are formed from m-cresol released during biomass combustion and diesel exhaust (Kourtchev et al., 2016). These tracers also exhibit the same strong correlation of 0.97 with this factor (Table S8). Syringic acid ($C_9H_{10}O_5$) also correlates well ($R = 0.70$) with this factor. In terms of its daily cycle did not show peaks during morning or evening rush hours; instead, a peak was observed around 20:00 LT, suggesting it aligns more with BBOA. This factor showed a strong correlation with highly oxidized nitrogen-containing compounds and secondary organic aerosols (syringic acid). This factor is more related to highly oxidized nitrogen-containing secondary organic aerosols, indicating that nitrogen-containing compounds produced by BBOA may have undergone significant oxidation by NO3 radicals. Therefore, I identified it as night-time aged BBOA.

The second factor was characterized by a high fraction of oleic acid $C_{18}H_{35}O_2^+$ ($R = 0.90$), $C_{16}H_{35}O_3^+$ ($C_{16}H_{33}O_2(H_2O)^+$) ($R = 0.88$), $C_{16}H_{33}O_2^+$ corresponding to palmitic acid ($R = 0.54$), and $C_{16}H_{31}O_1^+$ is the fragment of $C_{16}H_{33}O_2^+$ ($R = 0.54$). $C_{18}H_{34}O_2$ is identified as the cooking tracer oleic acid, while $C_{16}H_{33}O_2^+$ serves as another cooking aerosol tracer, corresponding to palmitic acid (Reyes-Villegas et al., 2018; Wang et al., 2020b; Huang et al., 2021). $C_{16}H_{31}O_1^+$ is thought to originate from $C_{16}H_{33}O_2^+$ due to fragmentation involving the loss of one H_2O molecule. These findings strongly suggest that this factor represents cooking aerosol.

The third factor was identified as aged combustion. In this factor, the aromatic hydrocarbon $C_7H_9^+$ accounts for a relatively higher fraction and exhibits a strong correlation ($R = 0.79$). Although $C_8H_{13}^+$ does not contribute significantly as $C_7H_9^+$, it also shows the same strong correlation. These compounds are attributed to combustion sources (Wang et al., 2022). The ion $C_7H_{10}N_1^+$, potentially a fragment of acridine ($C_7H_{12}N_1^+$) originating from coal combustion (Wang

et al., 2021), exhibits a distinct signal and the highest correlation ($R = 0.94$). Similarly, $C_6H_{15}?O_3^+$ ($R = 0.93$) corresponds to 2-methoxyethyl ether (MXEE), a product of fuel combustion. Monoterpene oxidation products, such as $C_{10}H_{17}O_1^+$ ($R = 0.86$) and $C_9H_{13}?O_1^+$ ($R = 0.82$), are also observed. This is likely because monoterpenes, serving as biofuel components in engines and boilers, form oxidized monoterpene products when combusted and oxidized (Dagaut et al., 2024). Additionally, benzocaine $C_9?H_{12}?N_1?O_2^+?$ exhibits strong correlation ($R = 0.80$) with this factor and is likely a product of oxidized combustion processes.

The fourth factor has C_6 carboxylic acids ($C_6H_7O_5^+$) which is the phenol oxidation products with OH radicals in the low-NO_x system, and $C_7H_9O_5^+$ denoted as the guaiacol with OH adduct. Propanedioic acid ($C_3H_5O_4^+$), pentanedione ($C_4H_5O_3^+$), and 2-oxopentanedioic acid $C_5H_7O_4^+$ are fragments derived from the OH oxidation products of biomass burning VOC (BBVOC) such as guaiacol and syringol (Yee et al., 2013). Additionally, $C_6H_6O_2$ is an OH radical oxidation product from phenol. A higher fraction of 2,5-di-(hydroxymethyl)furan $C_6H_9O_3^+$ was observed, which may result from $C_6H_7O_2^+$ binding with a water molecule. These photochemical products, formed from BBVOC oxidation by OH radicals, confirm that this factor represents aged BBOA. All the aforementioned ions exhibit a strong correlation of approximately 0.85 with this factor, as shown in Table S2. Furthermore, its diurnal pattern, with a peak at 15:00 LT during the day, leads to its identification as day-time aged BBOA.

The fifth factor shows a very strong correlation with stearic acid $C_{18}H_{37}O_2^+$ ($R = 0.95$), $C_{16}H_{33}O_2(H_2O)^+$ ($R = 0.91$), $C_{18}H_{15}O_1^+$ ($R = 0.90$), $C_{19}H_{15}O_1$ ($R = 0.88$), and oleic acid $C_{18}H_{35}O_2^+$ ($R = 0.88$). However, these compounds do not account for significant fractions in this factor's mass spectrum as they do in factor 2's mass spectrum. Notably, trimethoxy methane $C_4H_{11}O_3^+$ is a key ion in this factor but contributes minimally to others and shows no correlation with the factor ($R = 0.02$). While the composition includes unrelated compounds, its strong correlation with sulfate detected by AMS ($R = 0.74$) suggests a regional background origin, with the nighttime peak indicating local accumulation effects.

During summer, the composition of SVOA includes 11 ± 15 % weakly OBOA, 16 ± 15 % oxidized isoprene and BBOA (mixture of oxidized isoprene OA and BBOA), 25 ± 21 % BBOA, 30 ± 22 % attributed to regional background sources, and 18 ± 16 % to More OBOA (Fig. 6). Although cooking-related SVOA ions were present during summer, the higher contribution of biogenic oxidation products in overlapping mass spectral regions likely reduced the statistical separability of a distinct cooking factor in the SVOC PMF analysis (Zhu et al., 2018; Coggon et al., 2024a). In winter, nighttime aged BBOA accounts for 10 ± 9 %, cooking OA contributes 4 ± 5 %, aged combustion OA makes up 9 ± 10 %, daytime aged BBOA constitutes the largest fraction at 55 ± 21 %,

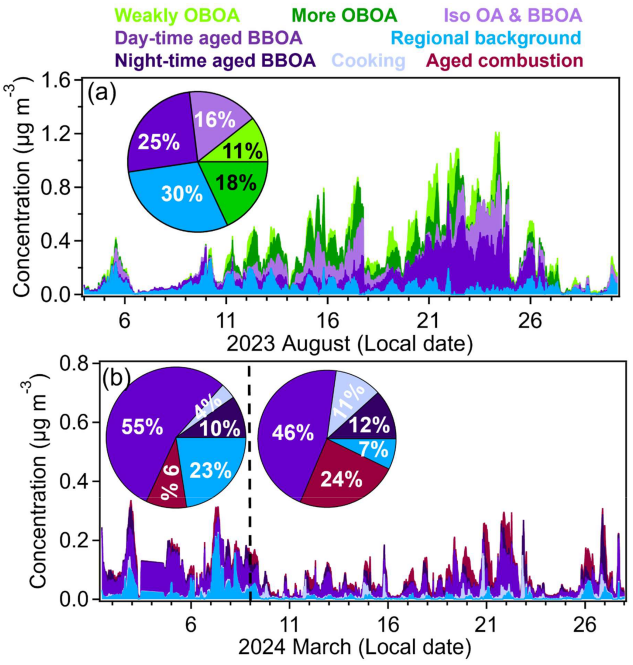

Figure 6. The time series and relative mass contributions (pie charts) of each SVOA factor to total SVOA concentrations in summer **(a)**, winter (left of the dash line), and spring (right of the dash line) **(b)**.

and regional background sources contribute 23 ± 17 %. In spring, nighttime aged BBOA accounts for 12 ± 12 %, cooking OA contributes 11 ± 12 %, aged combustion OA makes up 24 ± 18 %, daytime aged BBOA constitutes the largest fraction at 46 ± 25 %, and regional background sources contribute 7 ± 9 %.

3.2.3 Sources of organic aerosol particles

This study thoroughly examined source factor profiles, diurnal patterns, and correlations with tracers (Figs. S15–S20) for OA particles. The average organic aerosol concentration was $4.3 \pm 2.9\ \mu g\ m^{-3}$ in summer, $3.4 \pm 1.7\ \mu g\ m^{-3}$ in winter and $1.8 \pm 1.8\ \mu g\ m^{-3}$ in spring. Five OA factors were identified as the optimal interpretable solutions for summer and winter/spring, respectively. Alternative PMF solutions with different factor numbers were systematically evaluated based on Q/Q_{exp} behavior, factor interpretability, and tracer correlations; details are provided in the Supplement (Fig. S14).

In summer, the first factor was identified as cooking organic aerosol (COA), based on its high H : C ratio (1.82), low O : C ratio (0.19) (Fig. S17a), higher contributions at m/z 55 ($C_3H_3O^+$) and m/z 57 ($C_3H_5O^+$), and the mass spectrum dominated by hydrocarbon ions. These characteristics are consistent with reported COA in urban areas (Elser et al., 2016; Äijälä et al., 2017; Liu et al., 2018). Additionally, fatty acid ($C_{16}H_{35}O_3^+$) detected by CHARON-PTR showed a moderate correlation ($R = 0.54$) with the COA

time series (Fig. 17b). The second factor is characterized by a mass spectrum also dominated by hydrocarbon ions, a similar O : C ratio, and a high O : C ratio, but with higher contributions at m/z 55 ($C_4H_7^+$) and m/z 57 ($C_4H_9^+$) (Elser et al., 2016). These features are consistent with the characteristics of hydrocarbon-like organic aerosol (HOA) which is related to traffic. additionally, HOA shows a good correlation ($R = 0.66$) with the eBC time series. The third factor is assigned to Biogenic secondary organic aerosol (BOA), based on its H : C ratio of 1.63 and O : C of 0.44. The O / C ratio falls within the range typically associated with semi-volatile oxidized organic aerosol (SVOOA), which is approximately 0.35 ± 0.14 (Setyan et al., 2012). And it has a good correlation of 0.86 with monoterpene oxidation products (pinonaldehyde) in CHARON-PTR. BOA's diurnal pattern (Fig. S17c) shows an increase starting at 20:00 LT, reaching its peak at 07:00 LT. This trend aligns with the nighttime oxidation process of monoterpenes, supporting its identification as BOA. The fourth factor was identified as aged biomass burning organic aerosol (BBOA) because its O / C ratio of 0.597 is slightly higher than that of fresh BBOA (0.15–0.5) and falls within the range of aged BBOA (0.5–0.87) (Ortega et al., 2013). Its diurnal shows a small peak at 15:00 LT and a higher peak at 22:00 LT, the nighttime peak indicates that fresh BBOA happened rapid dark aging process (Kodros et al., 2020). And it shows a strong correlation ($R = 0.93$) with BBOA tracer levoglucosan detected by CHARON-PTR. therefore, the fourth factor is identified as aged BBOA. The fifth factor has the lowest H : C ratio (1.43) and the highest O : C ratio 0.75, which falls within the range of low-volatility oxygenated organic aerosol (LVOOA) (0.6–1.0) (Jimenez et al., 2009). LVOOA is dominated by CO^+ and CO_2^+ and shows a strong correlation ($R = 0.70$) with O_3, indicating that it is associated with photochemical oxidation processes (Kumar et al., 2016). Its diurnal pattern shows a daytime peak. These characteristics align well with the typical properties of LVOOA, leading to its identification as LVOOA. To ensure that every tracer detected by CHARON-PTR and correlated with AMS-PMF factors is representative, we compared different related fatty acids, toluene and trimethyl benzene, different monoterpene oxidation products, and different BBOA tracers. All of them showed good time-series correlations (Fig. S19).

In winter, we identified all the factors using the same method as in summer. The difference is that the traffic diurnal cycle (Fig. S18c) exhibits distinct peaks during the morning and evening rush hours. Fresh BBOA shows an evening peak, indicating evening residual heating activities. Aged BBOA is characterized by its correlation with $C_6H_7O_5^+$, which we identified as an oxidation product of BBOA in the CHARON-PTR section. its diurnal pattern is very flat, suggesting it may be associated with regional background levels or long-range transport. for LVOOA, NH_4^+ is used as an indicator, as it correlates strongly with inorganic aerosol during autumn and winter (Freney et al., 2011). Other different OA factors time series shown in Fig. S20.

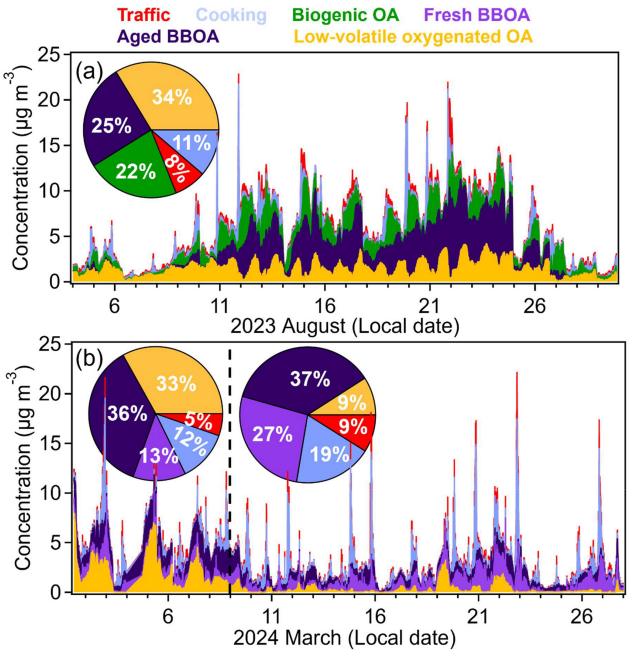

Figure 7. The time series and relative mass contributions (pie charts) of each OA factor to total OA concentrations in summer **(a)**, winter (left of the dash line), and spring (right of the dash line) **(b)**.

In summer, OA contributions are as follows: traffic 8 ± 8 %, cooking 11 ± 13 %, BOA 22 ± 14 %, aged BBOA 25 ± 21 %, and LVOOA 33 ± 20 %. In winter, the contributions are: traffic 5 ± 4 %, cooking 12 ± 12 %, fresh BBOA 13 ± 9 %, aged BBOA 36 ± 12 %, and LVOOA 33 ± 17 %. In spring, the contributions are: traffic 9 ± 7 %, cooking 19 ± 16 %, fresh BBOA 27 ± 17 %, aged BBOA 37 ± 19 %, and LVOOA 9 ± 10 % (Fig. 7).

Previous PMF studies in Stuttgart and Karlsruhe identified consistent summer source patterns: traffic-related OA contributes less than 10 %, SV-OOA accounts for approximately 16 %, while LV-OOA dominates at around 75 % of OA mass. This LV-OOA prevalence indicates strong biogenic influence from regional vegetation and photochemical processes enhanced by higher summer temperatures. In Stuttgart, elevated winter $PM_{2.5}$ stems primarily from biomass burning and residential heating, evidenced by enhanced levoglucosan and nitrated phenol signals, alongside increased traffic-related primary OA (POA). Both traffic OA and BBOA contribute substantially, though LV-OOA remains significant. Karlsruhe experiences similar source patterns with increased residential heating, traffic emissions, and coal combustion from industrial sources, but benefits from less severe inversion and stagnation conditions, resulting in lower overall concentrations. Munich's intermediate winter pollution levels suggest a source composition transitioning between these profiles, warranting detailed PMF analysis to characterize its specific

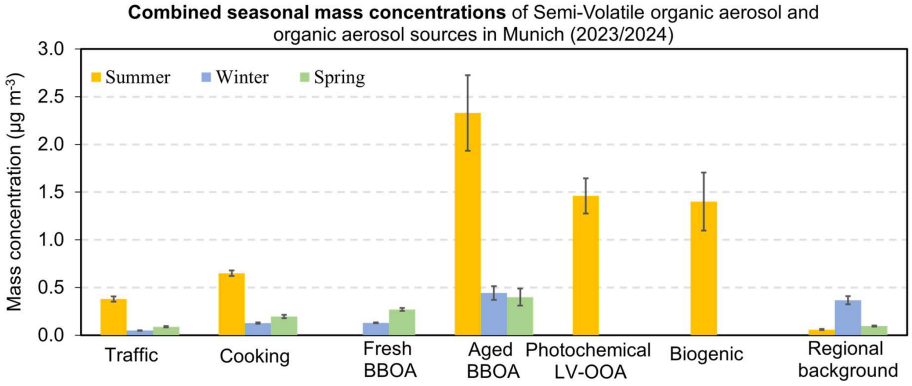

Figure 8. Comprehensive seasonal mass contributions of SVOA and OA sources in Munich summer, winter and spring time (Source categories combine factors from Charon-PTR-MS and HR-TOF-AMS: Aged BBOA (day-time aged BBOA, night-time aged BBOA, and IsoOA and BBOA from Charon; aged BBOA from AMS), Biogenic OA (weakly OBOA and More OBOA from Charon; BOA from AMS), with remaining sources combined similarly). Please note, that the total OA concentrations were $4.3 \pm 2.9\,\mu g\,m^{-3}$ in summer, $3.4 \pm 1.7\,\mu g\,m^{-3}$ in winter, and $1.8 \pm 1.8\,\mu g\,m^{-3}$ in spring.

emission contributions and compare with the established patterns in Stuttgart and Karlsruhe.

PMF source apportionment reveals strong seasonal dependencies in organic aerosol composition, with summer conditions driving the majority of aerosol burden in Munich. Summer demonstrates the highest concentrations across all source categories, dominated by aged BBOA ($2.3\,\mu g\,m^{-3}$) as the largest single contributor due to barbeque charcoal combustion. Photochemical LV-OOA ($1.5\,\mu g\,m^{-3}$) and biogenic emissions ($1.4\,\mu g\,m^{-3}$) emerge exclusively during summer, reflecting enhanced secondary aerosol formation under high temperatures and intense solar radiation that promote both biogenic emissions and photochemical processing. In contrast, late winter and spring show dramatically reduced organic aerosol levels, with late winter contributions limited primarily to regional background ($0.4\,\mu g\,m^{-3}$) and minimal aged BBOA ($0.4\,\mu g\,m^{-3}$). Traffic and cooking emissions remain consistently minor throughout all seasons ($\leq 0.7\,\mu g\,m^{-3}$), suggesting these local primary sources are less significant compared to secondary formation processes and regional biomass burning influences.

SVOA and OA composition exhibits distinct seasonal patterns driven by varying source emissions and atmospheric processing. Summer periods show elevated OA concentrations due to enhanced photochemical oxidation under high solar radiation, promoting secondary organic aerosol formation (Fig. 8). Biogenic sources contribute significantly during summer through increased vegetation emissions. Rapid atmospheric oxidation transforms fresh BBOA to aged BBOA, explaining the predominance of aged BBOA despite active barbecue activities. In late winter, residential heating dominated fresh BBOA emissions. During early spring, both heating and barbecue emissions contributed to fresh BBOA, with the latter increasing as temperatures rose. Consequently, Fresh BBOA concentrations increased from late winter to early spring. However, Fresh BBOA became less detectable in peak summer due to accelerated aging processes under higher temperatures and enhanced photochemical activity. Late winter and spring show substantial aged BBOA from residential heating activities. Cooking and traffic emissions remain consistent year-round sources, though their oxidation efficiency increases significantly in summer compared to winter and early spring when photochemical processes are less active.

3.3 Seasonal strong biomass burning aerosol events

PMF analysis of AMS mass spectra reveals that aged BBOA substantially contributes to total OA with seasonal variations: $25 \pm 21\,\%$ in summer, $36 \pm 12\,\%$ in winter, and $37 \pm 19\,\%$ in spring. Two prominent BBOA events were observed during 22–24 August (OA: $7.9 \pm 1.7\,\mu g\,m^{-3}$) and 7–9 March (OA: $3.3 \pm 1.3\,\mu g\,m^{-3}$).

During August 2023, aged BBOA showed strong correlations with multiple biomass burning indicators (Fig. 9 and Table S10). The high correlation with eBC ($R = 0.75$) suggests significant light-absorbing carbon from combustion processes. Primary biomass burning tracers showed excellent correlations: levoglucosan ($C_6H_{11}O_5^+$, $R = 0.93$) and syringic acid ($C_9H_{11}O_5^+$, $R = 0.84$), confirming fresh biomass burning emissions. The strong correlation with atmospheric oxidation products such as $C_6H_7O_5^+$ ($R = 0.88$, phenol oxidation products from OH radical reactions under low-NO_x conditions) and $C_7H_9O_5^+$ ($R = 0.87$, guaiacol-OH oxidation products) indicates significant photochemical aging processes during summer. Notably, aged BBOA correlated strongly with barbecue charcoal combustion tracers including formaldehyde ($R = 0.80$) (Kabir et al., 2010), coniferyl alcohol ($C_{10}H_{13}O_3^+$, $R = 0.90$), pinic acid ($C_9H_{15}O_4^+$, $R = 0.76$), and homovanilic acid ($C_9H_{11}O_4^+$, $R = 0.83$) (Vicente

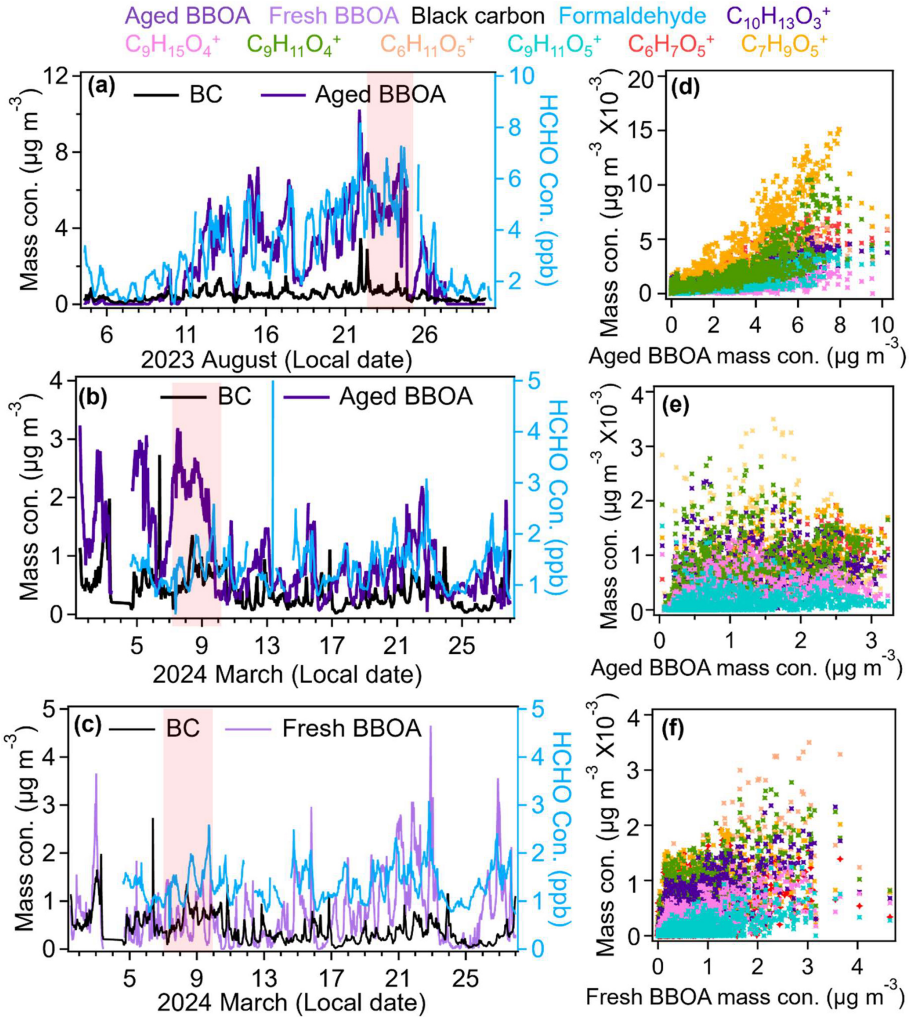

Figure 9. Time series of aged BBOA, black carbon, and formaldehyde during summer (August 2023, **a**) and winter/spring (March 2024, **b**) periods and fresh BBOA during March 2024 **(c)**; scatter plots showing correlations between aged BBOA and barbecue charcoal combustion tracers ($C_{10}H_{13}O_3^+$, $C_9H_{15}O_4^+$, $C_9H_{11}O_4^+$), and biomass burning tracers ($C_6H_{11}O_5^+$, $C_9H_{11}O_5^+$, $C_9H_7O_3^+$, $C_6H_7O_5^+$, $C_7H_9O_5^+$) in summer **(d)**, in winter **(e)** and Fresh BBOA correlated with all the tracers **(f)**. Strong BBOA events are in red shade.

et al., 2018). Several of these tracers are considered more specific to charcoal combustion than to traffic or fossil-fuel sources, and the pronounced evening maximum of the factor is consistent with typical barbecue activity patterns, supporting a local grilling-related origin. Backward trajectory analysis combined with VIIRS fire radiative power (FRP) data for August suggests negligible influence from regional wildfires along the air-mass transport pathways (Fig. S21a). Although several fire detections classified as "unknown" sources were observed (Fig. S21b), their FRP values were very low, indicating weak fire intensity and suggesting that they are unlikely to contribute substantially to the elevated BBOA levels observed in Munich. However, during the intensive BBOA episode (22–24 August), most tracer correlations decreased slightly, and formaldehyde showed no correlation with aged BBOA ($R = -0.20$) in Table S10. This suggests that during high-concentration events, different source contributions alter the chemical fingerprint, possibly indicating the influence of additional fresh emissions or changes in atmospheric processing conditions. Back trajectory analysis during the strong BBOA event shows that 51 % of air masses originated from long-range transport near the Belgium border (average BBOA: 5.3 μg m^{-3}), while 15 % from the Bavarian region exhibited the highest concentrations (7.3 μg m^{-3}) in Fig. S22. Given the absence of wildfire sources and the strong correlations with barbeque charcoal combustion tracers, we attribute the elevated concentrations primarily to outdoor barbeque charcoal combustion emissions.

In the whole March 2024, aged BBOA exhibited markedly different correlation patterns, indicating distinct sources and processes. The weaker correlation with eBC ($R = 0.39$) suggests different combustion characteristics compared to sum-

mer. Most importantly, aged BBOA showed poor correlations with barbecue charcoal combustion tracers: formaldehyde ($R = 0.14$), coniferyl alcohol ($R = 0.47$), pinic acid ($R = 0.41$), and homovanilic acid ($R = 0.51$). The dramatic decrease in these correlations compared to summer values indicate minimal contribution from outdoor cooking activities during winter months. Primary biomass burning markers also showed reduced correlations: levoglucosan ($R = 0.30$), and syringic acid ($C_9H_{11}O_5^+$, $R = 0.24$), suggesting different emission sources or processing pathways. Conversely, aged BBOA maintained strong correlations with guaiacol oxidation products: $C_6H_7O_5^+$ ($R = 0.80$) and $C_7H_9O_5^+$ ($R = 0.74$). This pattern strongly indicates that winter aged BBOA primarily originates from residential heating emissions that have undergone atmospheric oxidation (Kodros et al., 2020). The guaiacol derivatives are characteristic markers of wood combustion for heating purposes, and their predominant correlations with aged BBOA confirm this source attribution. In contrast, fresh BBOA showed strong correlations with barbecue charcoal combustion tracers: coniferyl alcohol ($R = 0.69$), pinic acid ($R = 0.68$), and homovanilic acid ($R = 0.67$), as well as primary biomass burning markers including levoglucosan ($R = 0.72$) and syringic acid ($R = 0.62$). Notably, fresh BBOA showed weak correlation with the aged oxidation products ($C_6H_7O_5^+$ and $C_7H_9O_5^+$) that strongly correlated with aged BBOA. This divergent correlation pattern suggests that fresh BBOA during late winter and early spring is associated with primary biomass-burning emissions, likely dominated by residential heating under weak photochemical conditions, with additional contributions from barbecue charcoal combustion as temperatures increase. Because these sources share similar biomass-burning signatures, a separation between residential heating and barbecue emissions has significant uncertainty. The observed separation between fresh and aged BBOA characteristics reflects slower atmospheric aging during colder periods compared to summer conditions, resulting in a clear separation between fresh and aged BBOA characteristics.

The intensive episode analysis (7–9 March 2024) revealed correlation patterns consistent with the monthly analysis (Table S10), reinforcing the conclusion that seasonal BBOA sources shift from barbecue charcoal combustions in summer to residential heating in winter. During this episode, aged BBOA maintained strong correlations exclusively with guaiacol oxidation products ($C_6H_7O_5^+$ and $C_7H_9O_5^+$), consistent with the monthly pattern. However, fresh BBOA exhibited notably selective correlations, showing moderate relationships only with coniferyl alcohol ($R = 0.65$) and levoglucosan ($R = 0.62$), while displaying weak or negligible correlations with other tracers. The limited correlation pattern of fresh BBOA can be attributed to its substantially lower concentration compared to aged BBOA during this period (Table S10). When aged BBOA dominates the total BBOA mass, the temporal variability of most tracers is primarily governed by the aged component, effectively masking the correlation signals from fresh BBOA. As a minor constituent, fresh BBOA's true relationships with various tracers become statistically obscured, making it challenging to establish robust correlations beyond the most characteristic primary emission markers (i.e., levoglucosan and coniferyl alcohol). This phenomenon highlights the importance of aged BBOA as the dominant source during winter heating periods, while fresh emissions represent localized, transient contributions that are rapidly diluted within the regional aged aerosol background. Back trajectory analysis reveals distinctly different transport patterns compared to summer. Winter air masses predominantly followed three clusters: Cluster 1 (32 %) transported through Czechia with BBOA concentrations of 2.3 $\mu g\,m^{-3}$, Cluster 2 (14 %) originating from Poland passing through Czechia (1.8 $\mu g\,m^{-3}$), and Cluster 3 (19 %) from the Belarus-Poland border passing through Czechia and Austria (1.1 $\mu g\,m^{-3}$) in Fig. S22. The dominance of Czechia-influenced trajectories (65 %) contrasts sharply with summer patterns, indicating significant contributions from Central European residential heating emissions. The prevalence of aged BBOA in these air masses suggests substantial accumulation of Aged BBOA during long-range transport. Notably, Cluster 2 exhibited elevated fresh BBOA concentrations, evidenced by lower O : C ratios, indicating recent biomass burning emissions from residential heating activities along the Polish transport pathway.

4 Conclusions

This study investigates the sources, concentrations, and seasonal variations of VOC, SVOA, and OA in an urban street canyon of the third largest German city, Munich, using a combination of online mass spectrometric observations and PMF based source apportionment. The results reveal a complex interplay between anthropogenic and biogenic sources, as well as atmospheric photochemical aging that governs the composition and evolution of the atmospheric pollutants in the urban street canyon.

The $PM_{2.5}$ analysis reveals Munich's distinctive air quality profile for different seasons. During summer, Munich's $PM_{2.5}$ concentrations ($6.7 \pm 3.7\,\mu g\,m^{-3}$) are comparable to neighboring German cities like Stuttgart ($7.1 \pm 3.3\,\mu g\,m^{-3}$) and Karlsruhe ($7.0 \pm 3.5\,\mu g\,m^{-3}$), also reflecting similar regional background conditions. Winter shows greater divergence: Munich's levels ($13.0 \pm 7.4\,\mu g\,m^{-3}$) exceed Karlsruhe's ($5.6 \pm 4.9\,\mu g\,m^{-3}$) but remain substantially lower than Stuttgart's pollution ($27.0 \pm 11.9\,\mu g\,m^{-3}$) also caused by stronger industrial sources in a basin like topography (Huang et al., 2019). This intermediate profile becomes even more significant when considering Munich's status as Germany's third-largest city, with a dense urban population and strong economic activity generating complex emission patterns, however, with less classical emissions from heavy industryCompared to other European cities – Paris with win-

ter $PM_{2.5}$ maximum of $15\,\mu g\,m^{-3}$, Berlin's winter $PM_{2.5}$ episodes above $15\,\mu g\,m^{-3}$ (the WHO, 2021 recommended daily limit), or Bern's winter $14\,\mu g\,m^{-3}$ average (Bressi et al., 2013; Grange et al., 2021; Renard et al., 2024) – Munich represents a critical test case with high population density, thriving industries and tourism.

Our findings identify and quantify a pronounced seasonal regime shift in organic aerosol composition. While a substantial anthropogenic baseline from traffic is persistent, the system transitions from a winter regime dominated by primary biomass burning aerosols (BBOA contributing up to 64 % of OA) to a summer regime governed by photochemical aging (LVOOA at 33 %) and formation of secondary biogenic aerosol. Critically, we demonstrate that biomass burning is not confined to the heating season. The significant and rising contribution from barbecue emissions in spring and summer reveals an underappreciated, health-sensitive emission source (Lenssen et al., 2022; Xu et al., 2023; Gruber and Kalamas, 2024).

The seasonal evolution of BBOA provides critical insights into its atmospheric processing. The presence of both fresh and aged BBOA in winter (fresh: 13 ± 9 %; aged: 36 ± 12 %) and spring (fresh: 27 ± 17 %; aged: 37 ± 19 %) contrasts sharply with the aerosol composition in summer, where only aged BBOA (25 ± 21 %) is detected. This pattern strongly indicates that primary biomass burning emissions undergo rapid atmospheric oxidation in summer, with substantial conversion to the aged type driven by enhanced photochemical activity (e.g., higher temperatures, radiation, and O3 levels). This rapid aging process for BBOA (Kodros et al., 2020; Li et al., 2023) presents a marked contrast to the typically slower, multi-generational oxidation pathway of anthropogenic VOCs from traffic (Srivastava et al., 2022), which require substantial atmospheric processing to form condensable SOA. A key implication of this finding is that if biomass burning OA persists in the atmosphere despite rapid aging processes, then mitigation strategies targeting primary biomass burning emissions could yield more immediate air quality benefits. We identified nocturnal oxidation of biogenic VOC as a significant SOA formation pathway in summer. The substantial contribution of biogenic VOCs (oxidized BVOC: 13 ± 13 %, and BVOC: 7 ± 7 %), coupled with BOA from oxidized monoterpenes (22 ± 14 %), demonstrates that nocturnal oxidation (primarily by O_3 and NO_3 radicals) generates secondary aerosol yields comparable those from daytime photochemical production (e.g., LVOOA at 33 ± 20 %). Consequently, monoterpene emission profiles must be treated as a critical air quality parameter and considered in urban vegetation management (Ren et al., 2014). It should be taken into account that the urban green can have positive but also negative impact on the levels of aerosol particles. Urban green infrastructure provides multiple environmental and health benefits, but may also influence secondary aerosol and ozone formation depending on species-specific BVOC emission characteristics (Ahn et al., 2022; Wang et al., 2025; Ma et al., 2025). For example, urban forestry programs can preferentially plant lower-monoterpene-emitting species such as Ginkgo biloba or Taxus cuspidata instead of high-emitting conifers such as Metasequoia glyptostroboides in NOx-rich street canyons, or adjust pruning and replacement strategies accordingly, which may help balance air-quality impacts while preserving ecosystem benefits (Maison et al., 2024).

Previous studies in Stuttgart and Karlsruhe (Huang et al., 2019; Song et al., 2022; Zhang et al., 2024) identified traffic-related OA contributions consistently at or below 10 % during summer. Munich exhibits similar patterns, with traffic OA contributing 8 ± 8 % in summer, 5 ± 4 % in winter, and 9 ± 7 % in spring. This consistency across all three cities in southwest Germany indicates that traffic is a minor OA component, exhibiting only relatively small seasonal variations. The most significant difference emerges in the abundance of LV-OOA. In Stuttgart and Karlsruhe, LV-OOA dominates summer OA with approximately 75 %, reflecting strong biogenic influence from regional vegetation and photochemical processes enhanced by higher temperatures. In contrast, Munich's LV-OOA remains substantially lower and relatively stable for different seasons (33 ± 20 % summer, 33 ± 17 % winter, 9 ± 10 % spring), indicating either reduced biogenic precursor emissions or weaker photochemical oxidation despite comparable regional conditions. In Stuttgart, elevated winter $PM_{2.5}$ stems primarily from biomass burning and residential heating, evidenced by enhanced levoglucosan and nitrated phenol signals. Both traffic OA and BBOA contribute substantially to winter pollution. Karlsruhe exhibits similar patterns, with residential heating, traffic emissions, and coal combustion from industrial sources driving winter $PM_{2.5}$ increases. Munich's source profile diverges markedly from both cities. BBOA contributes substantially more to Munich's OA composition year-round compared to Stuttgart and Karlsruhe. Summer shows notable BBOA contribution (aged BBOA 25 ± 21 % combined with BOA 22 ± 14 %), and winter BBOA dominance increases dramatically (fresh BBOA 13 ± 9 % plus aged BBOA 36 ± 12 %). Spring displays the highest BBOA contribution (fresh BBOA 27 ± 17 % plus aged BBOA 37 ± 19 %), indicating sustained biomass burning influence extending beyond residential heating into recreational activities. This persistent, elevated BBOA signature distinguishes Munich as a BBOA-dominated system, contrasting with the LV-OOA-dominated profiles of Stuttgart and Karlsruhe, and suggests that biomass burning requires year-round mitigation strategies in Munich.

In summary, this work reveals the dynamic chemical evolution of urban aerosol. The interplay between primary emissions from heating and cooking, the relatively constant traffic baseline, and the seasonally-modulated photochemical and nocturnal monoterpene chemistry creates a complex but decipherable pollution phenotype. Future research should prioritize tracking the atmospheric evolution of key source markers (e.g., from barbecues especially in summer and spring)

to constrain their aging timescales and health-relevant properties. Integrating these process-level insights is paramount for refining air quality models like PALM-4U (Zhang et al., 2024; Resler et al., 2024; Samad et al., 2024) to accurately predict effectivity of measures to improve air quality in future urban scenarios.

Data availability. The data used in this study is available at the KIT data repository KITopen data (https://doi.org/10.35097/bs139dd72d5s0r6a, Li et al., 2026).

Supplement. The supplement related to this article is available online at https://doi.org/10.5194/acp-26-5813-2026-supplement.

Author contributions. FK, JC, and HS conceived the concept, planned, and organized the campaign. YXL did the AMS and PTR-MS measurements, analyzed most of the data and wrote the manuscript with contributions from all co-authors. HS planned and organized the measurements, took care of the particle number, size and additional trace gas measurements. HZ, SA, AW, JC and FK supported instrument set up and conducted lidar measurements. XS, YWL and FK checked and calibrated the instruments during the measurements. JBS, ZA, and JS contributed to data analysis. TL contributed to planning of the measurement campaign and reviewed the manuscript.

Competing interests. At least one of the (co-)authors is a member of the editorial board of *Atmospheric Chemistry and Physics*. The peer-review process was guided by an independent editor, and the authors also have no other competing interests to declare.

Disclaimer. Publisher's note: Copernicus Publications remains neutral with regard to jurisdictional claims made in the text, published maps, institutional affiliations, or any other geographical representation in this paper. The authors bear the ultimate responsibility for providing appropriate place names. Views expressed in the text are those of the authors and do not necessarily reflect the views of the publisher.

Acknowledgements. We gratefully acknowledge the support by the meteorological department of the Ludwig-Maximilians-University of Munich (Group of Bernhard Mayer) and especially Markus Garhammer. The support by the technical team (Group of Steffen Vogt) of the Institute of Meteorology and Climate Research Atmospheric Aerosol Research of the Karlsruhe Institute of Technology was extremely helpful.

Financial support. The China Scholarship Council (CSC) provided PhD scholarships for Yanxia Li and Xuefeng Shi. The KIT Graduate School for Climate and Environment (GRACE) supported Yanxia Li. The KIT funded the campaign in the program "Changing Earth – Sustaining our Future" of the Helmholtz Association. The campaign was partly funded by the Institute for Advanced Study, Technical University of Munich (grant no. 291763). The TUM authors are partly supported by ERC Consolidator Grant CoSense4Climate (grant no. 101089203) and Bavarian State Ministry of the Environment (grant no. TLK 01U-75487). Yaowei Li acknowledges partial support from the NOAA Climate and Global Change Postdoctoral Fellowship Program, administered by UCAR's Cooperative Programs for the Advancement of Earth System Science (CPAESS) under award no. NA23OAR4310383B.

The article processing charges for this open-access publication were covered by the Karlsruhe Institute of Technology (KIT).

Review statement. This paper was edited by Sara Lance and reviewed by two anonymous referees.

References

Ahn, J.-W., Dinh, T.-V., Park, S.-Y., Choi, I.-Y., Park, C.-R., and Son, Y.-S.: Characteristics of biogenic volatile organic compounds emitted from major species of street trees and urban forests, Atmos. Pollut. Res., 13, https://doi.org/10.1016/j.apr.2022.101470, 2022.

Äijälä, M., Heikkinen, L., Fröhlich, R., Canonaco, F., Prévôt, A. S. H., Junninen, H., Petäjä, T., Kulmala, M., Worsnop, D., and Ehn, M.: Resolving anthropogenic aerosol pollution types – deconvolution and exploratory classification of pollution events, Atmos. Chem. Phys., 17, 3165–3197, https://doi.org/10.5194/acp-17-3165-2017, 2017.

Äijälä, M., Daellenbach, K. R., Canonaco, F., Heikkinen, L., Junninen, H., Petäjä, T., Kulmala, M., Prévôt, A. S. H., and Ehn, M.: Constructing a data-driven receptor model for organic and inorganic aerosol – a synthesis analysis of eight mass spectrometric data sets from a boreal forest site, Atmos. Chem. Phys., 19, 3645–3672, https://doi.org/10.5194/acp-19-3645-2019, 2019.

Aiken, A. C., DeCarlo, P. F., Kroll, J. H., Worsnop, D. R., Huffman, J. A., Docherty, K. S., Ulbrich, I. M., Mohr, C., Kimmel, J. R., Sueper, D., Sun, Y., Zhang, Q., Trimborn, A., Northway, M., Ziemann, P. J., Canagaratna, M. R., Onasch, T. B., Alfarra, M. R., and Prevot, A. S. H.: O / C and OM / OC Ratios of Primary, Secondary, and Ambient Organic Aerosols with High-Resolution Time-of-Flight Aerosol Mass Spectrometry, Environ. Sci. Technol., 42, 4478–4485, 2008.

Belis, C. A., Larsen, B. R., Amato, F., El Haddad, I., Favez, O., Harrison, R. M., Hopke, P. K., Nava, S., Paatero, P., Prévôt, A., Quass, U., Vecchi, R., and Viana, M.: European Guide on Air Pollution Source Apportionment with Receptor Models, European Commission, Joint Research Centre, Institute for Environment and Sustainability, Publications Office of the European Union, Luxembourg, https://doi.org/10.2788/9307, 2013.

Borbon, A., Fontaine, H., Veillerot, M., Locoge, N., Galloo, J.-C., and Guillermo, R.: An investigation into the traffic-related fraction of isoprene at an urban location, Atmos. Environ., 35, 3749–3760, 2001.

Bressi, M., Sciare, J., Ghersi, V., Bonnaire, N., Nicolas, J. B., Petit, J. E., Moukhtar, S., Rosso, A., Mihalopoulos, N., and Féron, A.: A one-year comprehensive chemical characterisation of fine aerosol ($PM_{2.5}$) at urban, suburban and rural background sites in the region of Paris (France), Atmos. Chem. Phys., 13, 7825–7844, https://doi.org/10.5194/acp-13-7825-2013, 2013.

Bruns, E. A., Slowik, J. G., El Haddad, I., Kilic, D., Klein, F., Dommen, J., Temime-Roussel, B., Marchand, N., Baltensperger, U., and Prévôt, A. S. H.: Characterization of gas-phase organics using proton transfer reaction time-of-flight mass spectrometry: fresh and aged residential wood combustion emissions, Atmos. Chem. Phys., 17, 705–720, https://doi.org/10.5194/acp-17-705-2017, 2017.

Canagaratna, M. R., Jayne, J. T., Jimenez, J. L., Allan, J. D., Alfarra, M. R., Zhang, Q., Onasch, T. B., Drewnick, F., Coe, H., Middlebrook, A., Delia, A., Williams, L. R., Trimborn, A. M., Northway, M. J., DeCarlo, P. F., Kolb, C. E., Davidovits, P., and Worsnop, D. R.: Chemical and microphysical characterization of ambient aerosols with the aerodyne aerosol mass spectrometer, Mass Spectrom. Rev., 26, 185–222, https://doi.org/10.1002/mas.20115, 2007.

Canagaratna, M. R., Jimenez, J. L., Kroll, J. H., Chen, Q., Kessler, S. H., Massoli, P., Hildebrandt Ruiz, L., Fortner, E., Williams, L. R., Wilson, K. R., Surratt, J. D., Donahue, N. M., Jayne, J. T., and Worsnop, D. R.: Elemental ratio measurements of organic compounds using aerosol mass spectrometry: characterization, improved calibration, and implications, Atmos. Chem. Phys., 15, 253–272, https://doi.org/10.5194/acp-15-253-2015, 2015.

Chakraborty, A., Tripathi, S. N., and Gupta, T.: Effects of organic aerosol loading and fog processing on organic aerosol volatility, J. Aerosol Sci., 105, 73–83, https://doi.org/10.1016/j.jaerosci.2016.11.015, 2017.

Chen, G., Canonaco, F., Slowik, J. G., Daellenbach, K. R., Tobler, A., Petit, J. E., Favez, O., Stavroulas, I., Mihalopoulos, N., Gerasopoulos, E., El Haddad, I., Baltensperger, U., and Prevot, A. S. H.: Real-Time Source Apportionment of Organic Aerosols in Three European Cities, Environ. Sci. Technol., 56, 15290–15297, https://doi.org/10.1021/acs.est.2c02509, 2022a.

Chen, G., Canonaco, F., Tobler, A., Aas, W., Alastuey, A., Allan, J., Atabakhsh, S., Aurela, M., Baltensperger, U., Bougiatioti, A., De Brito, J. F., Ceburnis, D., Chazeau, B., Chebaicheb, H., Daellenbach, K. R., Ehn, M., El Haddad, I., Eleftheriadis, K., Favez, O., Flentje, H., Font, A., Fossum, K., Freney, E., Gini, M., Green, D. C., Heikkinen, L., Herrmann, H., Kalogridis, A. C., Keernik, H., Lhotka, R., Lin, C., Lunder, C., Maasikmets, M., Manousakas, M. I., Marchand, N., Marin, C., Marmureanu, L., Mihalopoulos, N., Mocnik, G., Necki, J., O'Dowd, C., Ovadnevaite, J., Peter, T., Petit, J. E., Pikridas, M., Matthew Platt, S., Pokorna, P., Poulain, L., Priestman, M., Riffault, V., Rinaldi, M., Rozanski, K., Schwarz, J., Sciare, J., Simon, L., Skiba, A., Slowik, J. G., Sosedova, Y., Stavroulas, I., Styszko, K., Teinemaa, E., Timonen, H., Tremper, A., Vasilescu, J., Via, M., Vodicka, P., Wiedensohler, A., Zografou, O., Cruz Minguillon, M., and Prevot, A. S. H.: European aerosol phenomenology – 8: Harmonised source apportionment of organic aerosol using 22 Year-long ACSM/AMS datasets, Environ. Int., 166, 107325, https://doi.org/10.1016/j.envint.2022.107325, 2022b.

Chen, J.: Unique real-time sensor network for densely monitoring air pollutants in Munich, Technical University of Munich, https://www.ee.cit.tum.de/en/esm/forschung/air-pollutant-monitoring/ (last access: 20 November 2025), 2025.

Coggon, M. M., Stockwell, C. E., Xu, L., Peischl, J., Gilman, J. B., Lamplugh, A., Bowman, H. J., Aikin, K., Harkins, C., Zhu, Q., Schwantes, R. H., He, J., Li, M., Seltzer, K., McDonald, B., and Warneke, C.: Contribution of cooking emissions to the urban volatile organic compounds in Las Vegas, NV, Atmos. Chem. Phys., 24, 4289–4304, https://doi.org/10.5194/acp-24-4289-2024, 2024a.

Coggon, M. M., Stockwell, C. E., Claflin, M. S., Pfannerstill, E. Y., Xu, L., Gilman, J. B., Marcantonio, J., Cao, C., Bates, K., Gkatzelis, G. I., Lamplugh, A., Katz, E. F., Arata, C., Apel, E. C., Hornbrook, R. S., Piel, F., Majluf, F., Blake, D. R., Wisthaler, A., Canagaratna, M., Lerner, B. M., Goldstein, A. H., Mak, J. E., and Warneke, C.: Identifying and correcting interferences to PTR-ToF-MS measurements of isoprene and other urban volatile organic compounds, Atmos. Meas. Tech., 17, 801–825, https://doi.org/10.5194/amt-17-801-2024, 2024b.

Crippa, M., DeCarlo, P. F., Slowik, J. G., Mohr, C., Heringa, M. F., Chirico, R., Poulain, L., Freutel, F., Sciare, J., Cozic, J., Di Marco, C. F., Elsasser, M., Nicolas, J. B., Marchand, N., Abidi, E., Wiedensohler, A., Drewnick, F., Schneider, J., Borrmann, S., Nemitz, E., Zimmermann, R., Jaffrezo, J. L., Prévôt, A. S. H., and Baltensperger, U.: Wintertime aerosol chemical composition and source apportionment of the organic fraction in the metropolitan area of Paris, Atmos. Chem. Phys., 13, 961–981, https://doi.org/10.5194/acp-13-961-2013, 2013.

Daellenbach, K. R., Kourtchev, I., Vogel, A. L., Bruns, E. A., Jiang, J., Petäjä, T., Jaffrezo, J.-L., Aksoyoglu, S., Kalberer, M., Baltensperger, U., El Haddad, I., and Prévôt, A. S. H.: Impact of anthropogenic and biogenic sources on the seasonal variation in the molecular composition of urban organic aerosols: a field and laboratory study using ultra-high-resolution mass spectrometry, Atmos. Chem. Phys., 19, 5973–5991, https://doi.org/10.5194/acp-19-5973-2019, 2019.

Dagaut, P., Dbouk, Z., Belhadj, N., Lailliau, M., and Benoit, R.: On the combustion of terpenes biofuels, in: ASME Turbo Expo 2024: Turbomachinery Technical Conference and Exposition, London, UK, https://doi.org/10.1115/GT2024-121549, 2024.

Debevec, C., Sauvage, S., Gros, V., Salameh, T., Sciare, J., Dulac, F., and Locoge, N.: Seasonal variation and origins of volatile organic compounds observed during 2 years at a western Mediterranean remote background site (Ersa, Cape Corsica), Atmos. Chem. Phys., 21, 1449–1484, https://doi.org/10.5194/acp-21-1449-2021, 2021.

DeCarlo, P. F., Kimmel, J. R., Trimborn, A., Northway, M. J., Jayne, J. T., Aiken, A. C., Gonin, M., Fuhrer, K., Horvath, T., Docherty, K. S., Worsnop, D. R., and Jimenez, J. L.: Field-deployable, high-resolution, time-of-flight aerosol mass spectrometer, Anal. Chem., 78, 8281–8289, https://doi.org/10.1021/ac061249n, 2006.

Docherty, K. S., Aiken, A. C., Huffman, J. A., Ulbrich, I. M., DeCarlo, P. F., Sueper, D., Worsnop, D. R., Snyder, D. C., Peltier, R. E., Weber, R. J., Grover, B. D., Eatough, D. J., Williams, B. J., Goldstein, A. H., Ziemann, P. J., and Jimenez, J. L.: The 2005 Study of Organic Aerosols at Riverside (SOAR-1): instrumental intercomparisons and fine particle composition, Atmos.

Chem. Phys., 11, 12387–12420, https://doi.org/10.5194/acp-11-12387-2011, 2011.

Eichler, P., Müller, M., D'Anna, B., and Wisthaler, A.: A novel inlet system for online chemical analysis of semi-volatile submicron particulate matter, Atmos. Meas. Tech., 8, 1353–1360, https://doi.org/10.5194/amt-8-1353-2015, 2015.

Elser, M., Huang, R.-J., Wolf, R., Slowik, J. G., Wang, Q., Canonaco, F., Li, G., Bozzetti, C., Daellenbach, K. R., Huang, Y., Zhang, R., Li, Z., Cao, J., Baltensperger, U., El-Haddad, I., and Prévôt, A. S. H.: New insights into PM2.5 chemical composition and sources in two major cities in China during extreme haze events using aerosol mass spectrometry, Atmos. Chem. Phys., 16, 3207–3225, https://doi.org/10.5194/acp-16-3207-2016, 2016.

Fleming, L. T., Lin, P., Roberts, J. M., Selimovic, V., Yokelson, R., Laskin, J., Laskin, A., and Nizkorodov, S. A.: Molecular composition and photochemical lifetimes of brown carbon chromophores in biomass burning organic aerosol, Atmos. Chem. Phys., 20, 1105–1129, https://doi.org/10.5194/acp-20-1105-2020, 2020.

Freney, E. J., Sellegri, K., Canonaco, F., Boulon, J., Hervo, M., Weigel, R., Pichon, J. M., Colomb, A., Prévôt, A. S. H., and Laj, P.: Seasonal variations in aerosol particle composition at the puy-de-Dôme research station in France, Atmos. Chem. Phys., 11, 13047–13059, https://doi.org/10.5194/acp-11-13047-2011, 2011.

Gkatzelis, G. I., Tillmann, R., Hohaus, T., Müller, M., Eichler, P., Xu, K.-M., Schlag, P., Schmitt, S. H., Wegener, R., Kaminski, M., Holzinger, R., Wisthaler, A., and Kiendler-Scharr, A.: Comparison of three aerosol chemical characterization techniques utilizing PTR-ToF-MS: a study on freshly formed and aged biogenic SOA, Atmos. Meas. Tech., 11, 1481–1500, https://doi.org/10.5194/amt-11-1481-2018, 2018a.

Gkatzelis, G. I., Hohaus, T., Tillmann, R., Gensch, I., Müller, M., Eichler, P., Xu, K.-M., Schlag, P., Schmitt, S. H., Yu, Z., Wegener, R., Kaminski, M., Holzinger, R., Wisthaler, A., and Kiendler-Scharr, A.: Gas-to-particle partitioning of major biogenic oxidation products: a study on freshly formed and aged biogenic SOA, Atmos. Chem. Phys., 18, 12969–12989, https://doi.org/10.5194/acp-18-12969-2018, 2018b.

Gkatzelis, G. I., Coggon, M. M., McDonald, B. C., Peischl, J., Gilman, J. B., Aikin, K. C., Robinson, M. A., Canonaco, F., Prevot, A. S. H., Trainer, M., and Warneke, C.: Observations Confirm that Volatile Chemical Products Are a Major Source of Petrochemical Emissions in U.S. Cities, Environ. Sci. Technol., 55, 4332–4343, https://doi.org/10.1021/acs.est.0c05471, 2021.

Grange, S. K., Fischer, A., Zellweger, C., Alastuey, A., Querol, X., Jaffrezo, J.-L., Weber, S., Uzu, G., and Hueglin, C.: Switzerland's PM_{10} and $PM_{2.5}$ environmental increments show the importance of non-exhaust emissions, Atmos. Environ. X, 12, 100145, https://doi.org/10.1016/j.aeaoa.2021.100145, 2021.

Gruber, R. P. and Kalamas, N.: Current Concepts towards the Health Hazards of BBQ Smoke and Newer Possibilities for Risk Mitigation: A Pilot Study, J. Biomed. Res. Environ. Sci., 5, 675–682, https://doi.org/10.37871/jbres1942, 2024.

Guo, J., Zhang, J., Shao, J., Chen, T., Bai, K., Sun, Y., Li, N., Wu, J., Li, R., Li, J., Guo, Q., Cohen, J. B., Zhai, P., Xu, X., and Hu, F.: A merged continental planetary boundary layer height dataset based on high-resolution radiosonde measurements, ERA5 reanalysis, and GLDAS, Earth Syst. Sci. Data, 16, 1–14, https://doi.org/10.5194/essd-16-1-2024, 2024.

Huang, D. D., Zhu, S., An, J., Wang, Q., Qiao, L., Zhou, M., He, X., Ma, Y., Sun, Y., Huang, C., Yu, J. Z., and Zhang, Q.: Comparative Assessment of Cooking Emission Contributions to Urban Organic Aerosol Using Online Molecular Tracers and Aerosol Mass Spectrometry Measurements, Environ. Sci. Technol., 55, 14526–14535, https://doi.org/10.1021/acs.est.1c03280, 2021.

Huang, W., Saathoff, H., Shen, X., Ramisetty, R., Leisner, T., and Mohr, C.: Seasonal characteristics of organic aerosol chemical composition and volatility in Stuttgart, Germany, Atmos. Chem. Phys., 19, 11687–11700, https://doi.org/10.5194/acp-19-11687-2019, 2019.

Huang, X.-F., Zou, B.-B., He, L.-Y., Hu, M., Prévôt, A. S. H., and Zhang, Y.-H.: Exploration of $PM_{2.5}$ sources on the regional scale in the Pearl River Delta based on ME-2 modeling, Atmos. Chem. Phys., 18, 11563–11580, https://doi.org/10.5194/acp-18-11563-2018, 2018.

IPCC: Climate Change 2023: Synthesis Report, in: Contribution of Working Groups I, II and III to the Sixth Assessment Report of the Intergovernmental Panel on Climate Change, IPCC, Geneva, Switzerland, https://doi.org/10.59327/IPCC/AR6-9789291691647, 2023.

Jain, V., Tripathi, S. N., Tripathi, N., Sahu, L. K., Gaddamidi, S., Shukla, A. K., Bhattu, D., and Ganguly, D.: Seasonal variability and source apportionment of non-methane VOCs using PTR-TOF-MS measurements in Delhi, India, Atmos. Environ., 283, https://doi.org/10.1016/j.atmosenv.2022.119163, 2022.

Jimenez, J. L., Canagaratna, M. R., Donahue, N. M., Prevot, A. S. H., Zhang, Q., Kroll, J. H., DeCarlo, P. F., Allan, J. D., Coe, H., Ng, N. L., Aiken, A. C., Docherty, K. S., Ulbrich, I. M., and Grieshop, A. P.: Evolution of organic aerosols in the atmosphere, Science, 326, 1525–1529, https://doi.org/10.1126/science.1180353, 2009.

Kabir, E., Kim, K. H., Ahn, J. W., Hong, O. F., and Sohn, J. R.: Barbecue charcoal combustion as a potential source of aromatic volatile organic compounds and carbonyls, J. Hazard. Mater., 174, 492–499, https://doi.org/10.1016/j.jhazmat.2009.09.079, 2010.

Kajos, M. K., Rantala, P., Hill, M., Hellén, H., Aalto, J., Patokoski, J., Taipale, R., Hoerger, C. C., Reimann, S., Ruuskanen, T. M., Rinne, J., and Petäjä, T.: Ambient measurements of aromatic and oxidized VOCs by PTR-MS and GC-MS: intercomparison between four instruments in a boreal forest in Finland, Atmos. Meas. Tech., 8, 4453–4473, https://doi.org/10.5194/amt-8-4453-2015, 2015.

Kim, E., Hopke, P. K., Larson, T. V., Maykut, N. N., and Lewtas, J.: Factor Analysis of Seattle Fine Particles, Aerosol Sci. Tech., 38, 724–738, https://doi.org/10.1080/02786820490490119, 2004.

Kodros, J. K., Papanastasiou, D. K., Paglione, M., Masiol, M., Squizzato, S., Florou, K., Skyllakou, K., Kaltsonoudis, C., Nenes, A., and Pandis, S. N.: Rapid dark aging of biomass burning as an overlooked source of oxidized organic aerosol, P. Natl. Acad. Sci. USA, 117, 33028–33033, https://doi.org/10.1073/pnas.2010365117, 2020.

Koss, A. R., Sekimoto, K., Gilman, J. B., Selimovic, V., Coggon, M. M., Zarzana, K. J., Yuan, B., Lerner, B. M., Brown, S. S., Jimenez, J. L., Krechmer, J., Roberts, J. M., Warneke, C., Yokelson, R. J., and de Gouw, J.: Non-methane organic gas

emissions from biomass burning: identification, quantification, and emission factors from PTR-ToF during the FIREX 2016 laboratory experiment, Atmos. Chem. Phys., 18, 3299–3319, https://doi.org/10.5194/acp-18-3299-2018, 2018.

Kourtchev, I., Godoi, R. H. M., Connors, S., Levine, J. G., Archibald, A. T., Godoi, A. F. L., Paralovo, S. L., Barbosa, C. G. G., Souza, R. A. F., Manzi, A. O., Seco, R., Sjostedt, S., Park, J.-H., Guenther, A., Kim, S., Smith, J., Martin, S. T., and Kalberer, M.: Molecular composition of organic aerosols in central Amazonia: an ultra-high-resolution mass spectrometry study, Atmos. Chem. Phys., 16, 11899–11913, https://doi.org/10.5194/acp-16-11899-2016, 2016.

Kumar, B., Chakraborty, A., Tripathi, S. N., and Bhattu, D.: Highly time resolved chemical characterization of submicron organic aerosols at a polluted urban location, Environ. Sci. Process. Imp., 18, 1285–1296, https://doi.org/10.1039/c6em00392c, 2016.

Kumar, V., Giannoukos, S., Haslett, S. L., Tong, Y., Singh, A., Bertrand, A., Lee, C. P., Wang, D. S., Bhattu, D., Stefenelli, G., Dave, J. S., Puthussery, J. V., Qi, L., Vats, P., Rai, P., Casotto, R., Satish, R., Mishra, S., Pospisilova, V., Mohr, C., Bell, D. M., Ganguly, D., Verma, V., Rastogi, N., Baltensperger, U., Tripathi, S. N., Prévôt, A. S. H., and Slowik, J. G.: Highly time-resolved chemical speciation and source apportionment of organic aerosol components in Delhi, India, using extractive electrospray ionization mass spectrometry, Atmos. Chem. Phys., 22, 7739–7761, https://doi.org/10.5194/acp-22-7739-2022, 2022.

Lalchandani, V., Kumar, V., Tobler, A., M. Thamban, N., Mishra, S., Slowik, J. G., Bhattu, D., Rai, P., Satish, R., Ganguly, D., Tiwari, S., Rastogi, N., Tiwari, S., Močnik, G., Prévôt, A. S. H., and Tripathi, S. N.: Real-time characterization and source apportionment of fine particulate matter in the Delhi megacity area during late winter, Sci. Total Environ., 770, https://doi.org/10.1016/j.scitotenv.2021.145324, 2021.

Lannuque, V., D'Anna, B., Kostenidou, E., Couvidat, F., Martinez-Valiente, A., Eichler, P., Wisthaler, A., Müller, M., Temime-Roussel, B., Valorso, R., and Sartelet, K.: Gas–particle partitioning of toluene oxidation products: an experimental and modeling study, Atmos. Chem. Phys., 23, 15537–15560, https://doi.org/10.5194/acp-23-15537-2023, 2023.

Leglise, J., Muller, M., Piel, F., Otto, T., and Wisthaler, A.: Bulk Organic Aerosol Analysis by Proton-Transfer-Reaction Mass Spectrometry: An Improved Methodology for the Determination of Total Organic Mass, O : C and H : C Elemental Ratios, and the Average Molecular Formula, Anal. Chem., 91, 12619–12624, https://doi.org/10.1021/acs.analchem.9b02949, 2019.

Lemieux, P. M., Lutes, C. C., and Santoianni, D. A.: Emissions of organic air toxics from open burning: a comprehensive review, Progr. Energ. Combust. Sci., 30, 1–32, https://doi.org/10.1016/j.pecs.2003.08.001, 2004.

Lenssen, E. S., Pieters, R. H. H., Nijmeijer, S. M., Oldenwening, M., Meliefste, K., and Hoek, G.: Short-term associations between barbecue fumes and respiratory health in young adults, Environ. Res., 204, 111868, https://doi.org/10.1016/j.envres.2021.111868, 2022.

LfU Bayern: Messwertarchiv – Luftgütemessungen in Bayern, https://www.lfu.bayern.de/luft/immissionsmessungen/messwertarchiv/index.htm, last access: 29 September 2025.

Li, H., Riva, M., Rantala, P., Heikkinen, L., Daellenbach, K., Krechmer, J. E., Flaud, P.-M., Worsnop, D., Kulmala, M., Villenave, E., Perraudin, E., Ehn, M., and Bianchi, F.: Terpenes and their oxidation products in the French Landes forest: insights from Vocus PTR-TOF measurements, Atmos. Chem. Phys., 20, 1941–1959, https://doi.org/10.5194/acp-20-1941-2020, 2020a.

Li, S., Liu, D., Wu, Y., Hu, K., Jiang, X., Tian, P., Sheng, J., Pan, B., and Zhao, D.: Aging effects on residential biomass burning emissions under quasi-real atmospheric conditions, Environ. Pollut., 337, 122615, https://doi.org/10.1016/j.envpol.2023.122615, 2023.

Li, W., Wang, J., Qi, L., Yu, W., Nie, D., Shi, S., Gu, C., Ge, X., and Chen, M.: Molecular characterization of biomass burning tracer compounds in fine particles in Nanjing, China, Atmos. Environ., 240, https://doi.org/10.1016/j.atmosenv.2020.117837, 2020b.

Li, Y., Zhang, H., Shi, X., Li, Y., Abou-Rizk, S., Smith, J. B., An, Z., Wenzel, A., Song, J., Leisner, T., Keutsch, F., Chen, J., and Saathoff, H.: Dataset to Sources, concentrations, and seasonal variations of VOC and aerosol particles in downtown Munich in 2023/24, Karlsruhe Institute of Technology [data set], https://doi.org/10.35097/bs139dd72d5s0r6a, 2026.

Liu, T., Wang, Z., Wang, X., and Chan, C. K.: Primary and secondary organic aerosol from heated cooking oil emissions, Atmospheric Chemistry and Physics, 18, 11363-11374, 10.5194/acp-18-11363-2018, 2018.

Ma, J., Wang, S., Chen, G., Zhu, S., Wang, P., Chen, J., and Zhang, H.: Estimating emissions of biogenic volatile organic compounds from urban green spaces and their contributions to secondary pollution, Environ. Sci.: Atmos., 5, 129–141, https://doi.org/10.1039/d4ea00099d, 2025.

Maison, A., Lugon, L., Park, S.-J., Baudic, A., Cantrell, C., Couvidat, F., D'Anna, B., Di Biagio, C., Gratien, A., Gros, V., Kalalian, C., Kammer, J., Michoud, V., Petit, J.-E., Shahin, M., Simon, L., Valari, M., Vigneron, J., Tuzet, A., and Sartelet, K.: Significant impact of urban tree biogenic emissions on air quality estimated by a bottom-up inventory and chemistry transport modeling, Atmos. Chem. Phys., 24, 6011–6046, https://doi.org/10.5194/acp-24-6011-2024, 2024.

Malik, T. G., Sahu, L. K., Gupta, M., Mir, B. A., Gajbhiye, T., Dubey, R., Clavijo McCormick, A., and Pandey, S. K.: Environmental Factors Affecting Monoterpene Emissions from Terrestrial Vegetation, Plants, 12, https://doi.org/10.3390/plants12173146, 2023.

Massoli, P., Stark, H., Canagaratna, M. R., Krechmer, J. E., Xu, L., Ng, N. L., Mauldin, R. L., Yan, C., Kimmel, J., Misztal, P. K., Jimenez, J. L., Jayne, J. T., and Worsnop, D. R.: Ambient Measurements of Highly Oxidized Gas-Phase Molecules during the Southern Oxidant and Aerosol Study (SOAS) 2013, ACS Earth Space Chem., 2, 653–672, https://doi.org/10.1021/acsearthspacechem.8b00028, 2018.

Middlebrook, A. M., Bahreini, R., Jimenez, J. L., and Canagaratna, M. R.: Evaluation of Composition-Dependent Collection Efficiencies for the Aerodyne Aerosol Mass Spectrometer using Field Data, Aerosol Sci. Tech., 46, 258–271, https://doi.org/10.1080/02786826.2011.620041, 2012.

Molteni, U., Bianchi, F., Klein, F., El Haddad, I., Frege, C., Rossi, M. J., Dommen, J., and Baltensperger, U.: Formation of highly oxygenated organic molecules from aromatic compounds, Atmos. Chem. Phys., 18, 1909–1921, https://doi.org/10.5194/acp-18-1909-2018, 2018.

Müller, M., Mikoviny, T., Jud, W., D'Anna, B., and Wisthaler, A.: A new software tool for the analysis of high resolution PTR-TOF mass spectra, Chemometr. Intel. Labor. Syst., 127, 158–165, https://doi.org/10.1016/j.chemolab.2013.06.011, 2013.

Müller, M., Eichler, P., D'Anna, B., Tan, W., and Wisthaler, A.: Direct Sampling and Analysis of Atmospheric Particulate Organic Matter by Proton-Transfer-Reaction Mass Spectrometry, Anal. Chem., 89, 10889–10897, https://doi.org/10.1021/acs.analchem.7b02582, 2017.

München: LHM Stat. Faltkarte, https://stadt.muenchen.de/dam/jcr:ddaedd0e-0914-4093-b46a-5a62accc9bf9/LHM-StatTB_2023_DS.pdf?utm_source=chatgpt.com (last access: 23 April 2026), 2023.

Nakao, S., Clark, C., Tang, P., Sato, K., and Cocker Iii, D.: Secondary organic aerosol formation from phenolic compounds in the absence of NO_x, Atmos. Chem. Phys., 11, 10649–10660, https://doi.org/10.5194/acp-11-10649-2011, 2011.

Nault, B. A., Jo, D. S., McDonald, B. C., Campuzano-Jost, P., Day, D. A., Hu, W., Schroder, J. C., Allan, J., Blake, D. R., Canagaratna, M. R., Coe, H., Coggon, M. M., DeCarlo, P. F., Diskin, G. S., Dunmore, R., Flocke, F., Fried, A., Gilman, J. B., Gkatzelis, G., Hamilton, J. F., Hanisco, T. F., Hayes, P. L., Henze, D. K., Hodzic, A., Hopkins, J., Hu, M., Huey, L. G., Jobson, B. T., Kuster, W. C., Lewis, A., Li, M., Liao, J., Nawaz, M. O., Pollack, I. B., Peischl, J., Rappenglück, B., Reeves, C. E., Richter, D., Roberts, J. M., Ryerson, T. B., Shao, M., Sommers, J. M., Walega, J., Warneke, C., Weibring, P., Wolfe, G. M., Young, D. E., Yuan, B., Zhang, Q., de Gouw, J. A., and Jimenez, J. L.: Secondary organic aerosols from anthropogenic volatile organic compounds contribute substantially to air pollution mortality, Atmos. Chem. Phys., 21, 11201–11224, https://doi.org/10.5194/acp-21-11201-2021, 2021.

Niu, Y., Yan, Y., Li, J., Liu, P., Liu, Z., Hu, D., Peng, L., and Wu, J.: Establishment and verification of anthropogenic volatile organic compound emission inventory in a typical coal resource-based city, Environ. Pollut., 288, 117794, https://doi.org/10.1016/j.envpol.2021.117794, 2021.

Ortega, A. M., Day, D. A., Cubison, M. J., Brune, W. H., Bon, D., de Gouw, J. A., and Jimenez, J. L.: Secondary organic aerosol formation and primary organic aerosol oxidation from biomass-burning smoke in a flow reactor during FLAME-3, Atmos. Chem. Phys., 13, 11551–11571, https://doi.org/10.5194/acp-13-11551-2013, 2013.

Paatero, P.: The Multilinear Engine – A Table-Driven, Least Squares Program for Solving Multilinear Problems, Including then-Way Parallel Factor Analysis Model, J. Comput. Graph. Stat., 8, 854–888, https://doi.org/10.1080/10618600.1999.10474853, 1999.

Paatero, P. and Tapper, U.: Positive matrix factorization: A non-negative factor model with optimal utilization of error estimates of data values, Environmetrics, 5, 111–126, https://doi.org/10.1002/env.3170050203, 1994.

Peron, A., Graus, M., Striednig, M., Lamprecht, C., Wohlfahrt, G., and Karl, T.: Deciphering anthropogenic and biogenic contributions to selected non-methane volatile organic compound emissions in an urban area, Atmos. Chem. Phys., 24, 7063–7083, https://doi.org/10.5194/acp-24-7063-2024, 2024.

Pfannerstill, E. Y., Wang, N., Edtbauer, A., Bourtsoukidis, E., Crowley, J. N., Dienhart, D., Eger, P. G., Ernle, L., Fischer, H., Hottmann, B., Paris, J.-D., Stönner, C., Tadic, I., Walter, D., Lelieveld, J., and Williams, J.: Shipborne measurements of total OH reactivity around the Arabian Peninsula and its role in ozone chemistry, Atmos. Chem. Phys., 19, 11501–11523, https://doi.org/10.5194/acp-19-11501-2019, 2019.

Piel, F., Müller, M., Mikoviny, T., Pusede, S. E., and Wisthaler, A.: Airborne measurements of particulate organic matter by proton-transfer-reaction mass spectrometry (PTR-MS): a pilot study, Atmos. Meas. Tech., 12, 5947–5958, https://doi.org/10.5194/amt-12-5947-2019, 2019.

Pugliese, G., Piel, F., Trefz, P., Sulzer, P., Schubert, J. K., and Miekisch, W.: Effects of modular ion-funnel technology onto analysis of breath VOCs by means of real-time mass spectrometry, Anal. Bioanal. Chem., 412, 7131–7140, https://doi.org/10.1007/s00216-020-02846-8, 2020.

Qadir, R. M., Abbaszade, G., Schnelle-Kreis, J., Chow, J. C., and Zimmermann, R.: Concentrations and source contributions of particulate organic matter before and after implementation of a low emission zone in Munich, Germany, Environ. Pollut., 175, 158–167, https://doi.org/10.1016/j.envpol.2013.01.002, 2013.

Qi, L., Vogel, A. L., Esmaeilirad, S., Cao, L., Zheng, J., Jaffrezo, J.-L., Fermo, P., Kasper-Giebl, A., Daellenbach, K. R., Chen, M., Ge, X., Baltensperger, U., Prévôt, A. S. H., and Slowik, J. G.: A 1-year characterization of organic aerosol composition and sources using an extractive electrospray ionization time-of-flight mass spectrometer (EESI-TOF), Atmos. Chem. Phys., 20, 7875–7893, https://doi.org/10.5194/acp-20-7875-2020, 2020.

Reizer, M., Calzolai, G., Maciejewska, K., Orza, J. A. G., Carraresi, L., Lucarelli, F., and Juda-Rezler, K.: Measurement report: Receptor modeling for source identification of urban fine and coarse particulate matter using hourly elemental composition, Atmos. Chem. Phys., 21, 14471–14492, https://doi.org/10.5194/acp-21-14471-2021, 2021.

Ren, Y., Ge, Y., Gu, B., Min, Y., Tani, A., and Chang, J.: Role of management strategies and environmental factors in determining the emissions of biogenic volatile organic compounds from urban greenspaces, Environ. Sci. Technol., 48, 6237–6246, https://doi.org/10.1021/es4054434, 2014.

Renard, J.-B., Becker, G., Nodorft, M., Tavakoli, E., Thiele, L., Poincelet, E., Scholz, M., and Surcin, J.: High-Spatial Resolution Maps of $PM_{2.5}$ Using Mobile Sensors on Buses: A Case Study of Teltow City, Germany, in the Suburb of Berlin, 2023, Atmosphere, 15, 1494, https://doi.org/10.3390/atmos15121494, 2024.

Resler, J., Bauerová, P., Belda, M., Bureš, M., Eben, K., Fuka, V., Geletič, J., Jareš, R., Karel, J., Keder, J., Krč, P., Patiño, W., Radović, J., Řezníček, H., Sühring, M., Šindelářová, A., and Vlček, O.: Challenges of high-fidelity air quality modeling in urban environments – PALM sensitivity study during stable conditions, Geosci. Model Dev., 17, 7513–7537, https://doi.org/10.5194/gmd-17-7513-2024, 2024.

Reyes-Villegas, E., Green, D. C., Priestman, M., Canonaco, F., Coe, H., Prévôt, A. S. H., and Allan, J. D.: Organic aerosol source apportionment in London 2013 with ME-2: exploring the solution space with annual and seasonal analysis, Atmos. Chem. Phys., 16, 15545–15559, https://doi.org/10.5194/acp-16-15545-2016, 2016.

Reyes-Villegas, E., Bannan, T., Le Breton, M., Mehra, A., Priestley, M., Percival, C., Coe, H., and Allan, J. D.: Online Chemi-

cal Characterization of Food-Cooking Organic Aerosols: Implications for Source Apportionment, Environ. Sci. Technol., 52, 5308–5318, https://doi.org/10.1021/acs.est.7b06278, 2018.

Rios, J. C. R.: Atmospheric Chemistry of Isoprene Hydroxyhydroperoxides, PhD thesis, Department of Chemistry and Chemical Biology, Harvard University, Cambridge, USA, 159 pp., https://dash.harvard.edu/handle/1/42029714 (last access: 23 April 2026), 2018.

Riva, M., Budisulistiorini, S. H., Chen, Y., Zhang, Z., D'Ambro, E. L., Zhang, X., Gold, A., Turpin, B. J., Thornton, J. A., Canagaratna, M. R., and Surratt, J. D.: Chemical Characterization of Secondary Organic Aerosol from Oxidation of Isoprene Hydroxyhydroperoxides, Environ. Sci. Technol., 50, 9889–9899, https://doi.org/10.1021/acs.est.6b02511, 2016.

Romanias, M. N., Coggon, M. M., Al Ali, F., Burkholder, J. B., Dagaut, P., Decker, Z., Warneke, C., Stockwell, C. E., Roberts, J. M., Tomas, A., Houzel, N., Coeur, C., and Brown, S. S.: Emissions and Atmospheric Chemistry of Furanoids from Biomass Burning: Insights from Laboratory to Atmospheric Observations, ACS Earth Space Chem., 8, 857–899, https://doi.org/10.1021/acsearthspacechem.3c00226, 2024.

Samad, A., Caballero Arciénega, N. A., Alabdallah, T., and Vogt, U.: Application of the Urban Climate Model PALM-4U to Investigate the Effects of the Diesel Traffic Ban on Air Quality in Stuttgart, Atmosphere, 15, https://doi.org/10.3390/atmos15010111, 2024.

Schäfer, K., Stefan, E., Stefanie, S., Szabina, T., Balint, A., Janos, O., Mike, P., Christoph, Munkel, Josef Cyrys, Annette Peters, and Sarigiannis, D.: A measurement based analysis of the spatial distribution, temporal variation and chemical composition of particulate matter in Munich and Augsburg, Int. J. Tuberc. Lung Dis., 20, 047–057, https://doi.org/10.5588/ijtld.10.0498, 2011.

Schnell, F. I. J.: Aerosol distribution above Munich using remote sensing techniques, Dissertation LMU Munich, https://doi.org/10.5282/edoc.17368, 2014.

Schnelle-Kreis, J., Gebefügi, I., Welzl, G., Jaensch, T., and Kettrup, A.: Occurrence of particle-associated polycyclic aromatic compounds in ambient air of the city of Munich, Atmos. Environ., 35, S71–S81, https://doi.org/10.1016/S1352-2310(00)00557-4, 2001.

Seidler, J., Friedrich, M. N., Thomas, C. K., and Nölscher, A. C.: Introducing the novel concept of cumulative concentration roses for studying the transport of ultrafine particles from an airport to adjacent residential areas, Atmos. Chem. Phys., 24, 137–153, https://doi.org/10.5194/acp-24-137-2024, 2024.

Setyan, A., Zhang, Q., Merkel, M., Knighton, W. B., Sun, Y., Song, C., Shilling, J. E., Onasch, T. B., Herndon, S. C., Worsnop, D. R., Fast, J. D., Zaveri, R. A., Berg, L. K., Wiedensohler, A., Flowers, B. A., Dubey, M. K., and Subramanian, R.: Characterization of submicron particles influenced by mixed biogenic and anthropogenic emissions using high-resolution aerosol mass spectrometry: results from CARES, Atmos. Chem. Phys., 12, 8131–8156, https://doi.org/10.5194/acp-12-8131-2012, 2012.

Song, J., Saathoff, H., Gao, L., Gebhardt, R., Jiang, F., Vallon, M., Bauer, J., Norra, S., and Leisner, T.: Variations of $PM_{2.5}$ sources in the context of meteorology and seasonality at an urban street canyon in Southwest Germany, Atmos. Environ., 282, https://doi.org/10.1016/j.atmosenv.2022.119147, 2022.

Song, J., Saathoff, H., Jiang, F., Gao, L., Zhang, H., and Leisner, T.: Sources of organic gases and aerosol particles and their roles in nighttime particle growth at a rural forested site in southwest Germany, Atmos. Chem. Phys., 24, 6699–6717, https://doi.org/10.5194/acp-24-6699-2024, 2024.

Squires, F. A., Nemitz, E., Langford, B., Wild, O., Drysdale, W. S., Acton, W. J. F., Fu, P., Grimmond, C. S. B., Hamilton, J. F., Hewitt, C. N., Hollaway, M., Kotthaus, S., Lee, J., Metzger, S., Pingintha-Durden, N., Shaw, M., Vaughan, A. R., Wang, X., Wu, R., Zhang, Q., and Zhang, Y.: Measurements of traffic-dominated pollutant emissions in a Chinese megacity, Atmos. Chem. Phys., 20, 8737–8761, https://doi.org/10.5194/acp-20-8737-2020, 2020.

Srivastava, D., Vu, T. V., Tong, S., Shi, Z., and Harrison, R. M.: Formation of secondary organic aerosols from anthropogenic precursors in laboratory studies, npj Clim. Atmos. Sci., 5, https://doi.org/10.1038/s41612-022-00238-6, 2022.

Stein, A. F., Draxler, R. R., Rolph, G. D., Stunder, B. J. B., Cohen, M. D., and Ngan, F.: NOAA's HYSPLIT Atmospheric Transport and Dispersion Modeling System, B. Am. Meteorol. Soc., 96, 2059–2077, https://doi.org/10.1175/BAMS-D-14-00110.1, 2015.

Stirnberg, R., Cermak, J., Kotthaus, S., Haeffelin, M., Andersen, H., Fuchs, J., Kim, M., Petit, J.-E., and Favez, O.: Meteorology-driven variability of air pollution (PM_1) revealed with explainable machine learning, Atmos. Chem. Phys., 21, 3919–3948, https://doi.org/10.5194/acp-21-3919-2021, 2021.

Ulbrich, I. M., Canagaratna, M. R., Zhang, Q., Worsnop, D. R., and Jimenez, J. L.: Interpretation of organic components from Positive Matrix Factorization of aerosol mass spectrometric data, Atmos. Chem. Phys., 9, 2891–2918, https://doi.org/10.5194/acp-9-2891-2009, 2009.

Vicente, E. D., Vicente, A., Evtyugina, M., Carvalho, R., Tarelho, L. A. C., Oduber, F. I., and Alves, C.: Particulate and gaseous emissions from charcoal combustion in barbecue grills, Fuel Process. Technol., 176, 296–306, https://doi.org/10.1016/j.fuproc.2018.03.004, 2018.

Wan, X., Kawamura, K., Ram, K., Kang, S., Loewen, M., Gao, S., Wu, G., Fu, P., Zhang, Y., Bhattarai, H., and Cong, Z.: Aromatic acids as biomass-burning tracers in atmospheric aerosols and ice cores: A review, Environ. Pollut., 247, 216–228, https://doi.org/10.1016/j.envpol.2019.01.028, 2019.

Wang, H., Li, Y., Liu, Y., Lu, X., Zhang, Y., Fan, Q., Shen, C., Lai, S., Zhou, Y., Zhang, T., and Yue, D.: Underappreciated contributions of biogenic volatile organic compounds from urban green spaces to ozone pollution, Atmos. Chem. Phys., 25, 5233–5250, https://doi.org/10.5194/acp-25-5233-2025, 2025.

Wang, L., Slowik, J. G., Tripathi, N., Bhattu, D., Rai, P., Kumar, V., Vats, P., Satish, R., Baltensperger, U., Ganguly, D., Rastogi, N., Sahu, L. K., Tripathi, S. N., and Prévôt, A. S. H.: Source characterization of volatile organic compounds measured by proton-transfer-reaction time-of-flight mass spectrometers in Delhi, India, Atmos. Chem. Phys., 20, 9753–9770, https://doi.org/10.5194/acp-20-9753-2020, 2020a.

Wang, Q., He, X., Zhou, M., Huang, D. D., Qiao, L., Zhu, S., Ma, Y.-G., Wang, H.-L., Li, L., Huang, C., Huang, X. H. H., Xu, W., Worsnop, D., Goldstein, A. H., Guo, H., and Yu, J. Z.: Hourly Measurements of Organic Molecular Markers in Urban Shanghai, China: Primary Organic

Aerosol Source Identification and Observation of Cooking Aerosol Aging, ACS Earth Space Chem., 4, 1670–1685, https://doi.org/10.1021/acsearthspacechem.0c00205, 2020b.

Wang, W., Zhang, Y., Jiang, B., Chen, Y., Song, Y., Tang, Y., Dong, C., and Cai, Z.: Molecular characterization of organic aerosols in Taiyuan, China: Seasonal variation and source identification, Sci. Total Environ., 800, 149419, https://doi.org/10.1016/j.scitotenv.2021.149419, 2021.

Wang, Z., Wang, Z., Sun, J., Wang, Y., Sun, Z., Ma, K., and Wei, L.: Investigation of oxygen-enriched atmosphere combustion of oily sludge: Performance, mechanism, emission of the S/N-containing compound, and residue characteristics, J. Clean. Product., 378, https://doi.org/10.1016/j.jclepro.2022.134233, 2022.

Wenzel, A., Chen, J., Klama, T., Böhm, F., Angleitner, M., and Lobmaier, R.: Towards high-resolution air pollutants sensing through dense low-cost sensor networks – a case study in Munich, EGU General Assembly 2025, Vienna, Austria, 27 April–2 May 2025, https://doi.org/10.5194/egusphere-egu25-16784, 2025.

WHO – World Health Organization: The new 2021 WHO air quality guideline limits.Breeze Technologies Blog, https://www.breeze-technologies.de/blog/new-2021-who-air-quality-guideline-limits/ (last access: 23 April 2026), 2021.

Williams, L. R., Gonzalez, L. A., Peck, J., Trimborn, D., McInnis, J., Farrar, M. R., Moore, K. D., Jayne, J. T., Robinson, W. A., Lewis, D. K., Onasch, T. B., Canagaratna, M. R., Trimborn, A., Timko, M. T., Magoon, G., Deng, R., Tang, D., de la Rosa Blanco, E., Prévôt, A. S. H., Smith, K. A., and Worsnop, D. R.: Characterization of an aerodynamic lens for transmitting particles greater than 1 micrometer in diameter into the Aerodyne aerosol mass spectrometer, Atmos. Meas. Tech., 6, 3271–3280, https://doi.org/10.5194/amt-6-3271-2013, 2013.

Wu, C., Wang, C., Wang, S., Wang, W., Yuan, B., Qi, J., Wang, B., Wang, H., Wang, C., Song, W., Wang, X., Hu, W., Lou, S., Ye, C., Peng, Y., Wang, Z., Huangfu, Y., Xie, Y., Zhu, M., Zheng, J., Wang, X., Jiang, B., Zhang, Z., and Shao, M.: Measurement report: Important contributions of oxygenated compounds to emissions and chemistry of volatile organic compounds in urban air, Atmos. Chem. Phys., 20, 14769–14785, https://doi.org/10.5194/acp-20-14769-2020, 2020.

Wu, T., Müller, T., Wang, N., Byron, J., Langer, S., Williams, J., and Licina, D.: Indoor Emission, Oxidation, and New Particle Formation of Personal Care Product Related Volatile Organic Compounds, Environ. Sci. Technol. Lett., 11, 1053–1061, https://doi.org/10.1021/acs.estlett.4c00353, 2024.

Xu, C., Chen, J., Zhang, X., Cai, K., Chen, C., and Xu, B.: Emission characteristics and quantitative assessment of the health risks of cooking fumes during outdoor barbecuing, Environ. Pollut., 323, 121319, https://doi.org/10.1016/j.envpol.2023.121319, 2023.

Ye, Q., Krechmer, J. E., Shutter, J. D., Barber, V. P., Li, Y., Helstrom, E., Franco, L. J., Cox, J. L., Hrdina, A. I. H., Goss, M. B., Tahsini, N., Canagaratna, M., Keutsch, F. N., and Kroll, J. H.: Real-Time Laboratory Measurements of VOC Emissions, Removal Rates, and Byproduct Formation from Consumer-Grade Oxidation-Based Air Cleaners, Environ. Sci. Technol. Lett., 8, 1020–1025, https://doi.org/10.1021/acs.estlett.1c00773, 2021.

Yee, L. D., Kautzman, K. E., Loza, C. L., Schilling, K. A., Coggon, M. M., Chhabra, P. S., Chan, M. N., Chan, A. W. H., Hersey, S. P., Crounse, J. D., Wennberg, P. O., Flagan, R. C., and Seinfeld, J. H.: Secondary organic aerosol formation from biomass burning intermediates: phenol and methoxyphenols, Atmos. Chem. Phys., 13, 8019–8043, https://doi.org/10.5194/acp-13-8019-2013, 2013.

Yeoman, A. M., Shaw, M., Carslaw, N., Murrells, T., Passant, N., and Lewis, A. C.: Simplified speciation and atmospheric volatile organic compound emission rates from non-aerosol personal care products, Indoor Air, 30, 459–472, https://doi.org/10.1111/ina.12652, 2020.

Zhang, H., Huang, W., Shen, X., Ramisetty, R., Song, J., Kiseleva, O., Holst, C. C., Khan, B., Leisner, T., and Saathoff, H.: Aerosol composition, air quality, and boundary layer dynamics in the urban background of Stuttgart in winter, Atmos. Chem. Phys., 24, 10617–10637, https://doi.org/10.5194/acp-24-10617-2024, 2024.

Zhang, Q., Jimenez, J. L., Canagaratna, M. R., Ulbrich, I. M., Ng, N. L., Worsnop, D. R., and Sun, Y.: Understanding atmospheric organic aerosols via factor analysis of aerosol mass spectrometry: a review, Anal. Bioanal. Chem., 401, 3045–3067, https://doi.org/10.1007/s00216-011-5355-y, 2011.

Zhu, Q., Huang, X.-F., Cao, L.-M., Wei, L.-T., Zhang, B., He, L.-Y., Elser, M., Canonaco, F., Slowik, J. G., Bozzetti, C., El-Haddad, I., and Prévôt, A. S. H.: Improved source apportionment of organic aerosols in complex urban air pollution using the multilinear engine (ME-2), Atmos. Meas. Tech., 11, 1049–1060, https://doi.org/10.5194/amt-11-1049-2018, 2018.